Analysis of MD Trajectories as a Jump Diffusion Process: Butene Isomers in Zeolite Types TON and MEL

Fabien Jousse,* Laurence Leherte, and Daniel P. Vercauteren

Computational Chemical Physics Group, Facultés Universitaires Notre-Dame de la Paix, Rue de Bruxelles, 61, B-5000 Namur, Belgium

Received: January 29, 1997; In Final Form: March 27, 1997[⊗]

We have studied, by molecular dynamics, the self-diffusion of the four butene isomers in zeolite types TON and MEL at 623 K, for several loadings. Even if both systems present low-energy barriers to the diffusion (less than 10 kJ/mol), an essential difference appears between the two zeolite types. On one hand, TON presents unidirectional straight channels, and therefore there is almost no change of entropy during the migration of a guest molecule in the channel, so that their most probable position at 623 K corresponds to their minimum energy position. On the other hand, MEL presents intersecting straight channels, and while the minimum energy positions are located in the channels, the most probable positions are at the intersections, due to entropy effects which are larger than the energy change at 623 K. Using transition rate constants for site-to-site jumps estimated from the molecular dynamics trajectories, we have modeled the behavior of the four isomers of butene by a jump diffusion model (JDM). This appears to reproduce reasonably well their mean-square displacement in zeolite MEL, both at infinite dilution and at nonzero loading, due to the high free energy barriers attributed to the entropy effects. In zeolite TON, the self-diffusivities computed from a JDM are systematically underestimated as compared to those computed by molecular dynamics, due to the insufficient thermalization of the molecules. To better represent this diffusion mechanism, we have introduced a correlated jump diffusion model that accounts for insufficient thermalization by supposing that a given molecule has a larger probability to jump in the same direction as its previous jump than in the reverse direction. This correlated jump diffusion model reproduces well the diffusivity of *cis*-2-butene and isobutene in zeolite TON, but not that of *trans*-2-butene and 1-butene. The difference probably originates in the "fitting" of the guest molecules in the channels, as well as the guest−guest interactions.

1. Introduction

Zeolites are microporous materials whose regular structures present cavities or channels of molecular size (typically 4−8 Å).[1] The charge deficiencies of their aluminosilicate framework are compensated by metal cations or protons, which confer to these materials unique properties as sorbents, catalysts, or molecular sieves. Depending on the type of applications, their properties can be of different importance: the separation of N_2/O_2 in air mainly depends on the electric interactions with the zeolite cations,[2] while the activity for hydrocarbon isomerization reactions is mainly a function of the number and strength of the acid sites.[3] However, molecular diffusion is in general of major importance as it limits the rate with which a given guest molecule can travel within the crystallites, and therefore it can enhance or limit the zeolite activity in separation or catalytic processes. Therefore self-diffusion in zeolites and similar microporous materials is actively investigated,[4] experimentally as well as by theory or simulation.[5,6] It is a complex process, governed by multiple effects operating on different or similar time scales. Molecular dynamics (MD) simulations are used mainly to investigate the self-diffusivities of sorbed molecules in zeolites,[7] although it may also be used to study nonequilibrium transport properties.[8,9] Their investigations in zeolites are limited both by the duration of the simulations, which currently does not allow us to get reliable diffusivities less than about 10^{-6} m^2/s, and by the size of the model considered, which is usually too small to investigate the influence of spacially sparse events, such as defects or pore blocking. When low self-diffusivities originate in high energy barriers, those limitations can be overcome by using transition-state theory (TST).[10−13] The transition-state (TS) approximation allows simulation in the rare event regime, in which diffusion can be modeled as a series of uncorrelated jumps beween specific sites in the zeolite cavities or channels, such as cage-to-cage jumps in NaY.[12,13] The transition probabilities to jump from one site to another are evaluated by a Monte Carlo procedure, which allows us to determine directly the diffusion constant[11] or which can be used as input for dynamical Monte Carlo simulations.[12] The possible dynamical recrossings or multisite jumps can be accounted for by applying a dynamical correction factor computed through short MD runs starting at the transition state.[14,15] This TS approach using a dynamical correction factor agrees well with the MD simulations when these are feasible and give a much better estimation of the diffusivity in the rare event regime.

As a general rule, the assumption of uncorrelated jumps, which is central to TST, implies that the system presents high energy barriers to diffusion, as compared to kT; therefore, the molecules spend most of their time in given sites, where they thermalize before jumping to a neighboring site. The jumps are considered to be of infinitesimal duration, as compared with the residence time in a site. These assumptions allow to use a jump Monte Carlo model to study self-diffusion. Indeed, as this procedure greatly simplifies the calculations, events that take place on a much longer time scale can be investigated, such as the influence of defects of the crystallites, pore blocking,[16] or chemical reactions within the pores.[17] When systems present low energy barriers and when the molecules are less likely to thermalize between jumps, the applicability of a jump diffusion approach is however more problematic. Still, it has been shown by Hernández and Catlow in an MD

[⊗] Abstract published in *Advance ACS Abstracts,* May 15, 1997.

S1089-5647(97)00355-6 CCC: $14.00

simulation of *n*-butane and *n*-hexane in silicalite[18] that the diffusion could be considered as an activated process at room temperature for an activation energy as low as 4.4 kJ/mol, but they did not compare their results with the ones obtained by a jump diffusion model. Hence, to define more precisely the applicability of a JDM to systems with low energy barriers, we have studied by MD the self-diffusion of the four butene isomers in two zeolite types: TON (theta-1 or ZSM-22), which presents unidirectional channels along the crystallographic axis [001] and therefore is the simplest system in which we can study diffusion at infinite dilution; and MEL (ZSM-11 or silicalite-2), which presents a 3-dimensional network of interconnected identical channels running along [100] and [010].[19] These systems present a catalytic interest for butene skeletal or double-bond isomerization[20−24] and may also serve as model for similar systems. Indeed, while *trans*-2-butene and *cis*-2-butene are linear rigid molecules (the latter bulkier than the former), 1-butene is linear but flexible, and isobutene is rigid but plate-shaped, thus allowing us to investigate the influence of their shape and conformational properties on their self-diffusivities. We only considered the all-silica member in each zeolite family, which in both cases corresponds to existing materials.[25−28]

We have calculated, by a constrained energy minimization along the channels, that diffusion of butene in these channels is governed by energy barriers of about 10 kJ/mol, while our simulations were performed at 623 K, where $kT \approx 5.2$ kJ/mol. The computed self-diffusion coefficients can then be compared with those derived from a jump diffusion model, using rate constants derived from the MD calculations, both at infinite dilution and at finite loadings. In doing so, our aim was twofold: we wished to determine if the self-diffusion of the butene isomers in these zeolites can be considered as a jump diffusion process, to justify a further use of the simpler model of jump diffusion to study phenomena that occur on a longer time scale, such as the influence of pore blocking, defects, or chemical reactions; but we also wished to use the jump diffusion model as a tool for analyzing the MD trajectories using the concept of sites. We believe that this approach, which has been shown recently to give good results in the case of systems with high energy barriers,[13] can be very useful to investigate and elucidate the mechanism of the diffusion process. In the next section, we shortly summarize the computational tools used in the study. In section 3, we present the diffusion coefficients and vibrational density-of-states of the butene isomers in zeolite type TON; their mean-square displacement is then compared with the one computed from a JDM approach. Similar types of results obtained for diffusion of the butene isomers in zeolite type MEL are presented in Section 3b, for infinite dilution and at increasing loading, successively.

2. Computational Procedure

A. Molecular Dynamics. The MD simulations were performed in the NVT ensemble, with a fixed framework. Depending upon the number of molecules in the system, the duration of the runs varied between 60 and 200 ps. In all cases, we used the Discover 95.0 code of Biosym/MSI,[30] with the cff91_czeo force field,[31] which includes bonded interactions for the butene molecules and nonbonded interactions between the sorbed molecules, and between the molecules and the zeolite lattice. All atoms are considered in the calculation. Coulombic interactions were left out of the expression of the potential energy, as these were shown to barely influence the diffusion with this force field.[32] In all cases, the simulations were performed with a 1.0 fs time step. Typical MD runs lasted around 10^5 s on an IBM RS/6000 Model 560 workstation. Our MD simulations were performed with a rigid lattice. Hence, as the thermalization process originates from the collisions between the sorbed molecules and between the molecules and the zeolite lattice, we could not investigate the energy exchange between the molecules and the lattice vibrations, which has been shown to be faster than the energy exchange between the molecules.[8] However, this finding resulted from nonequilibrium MD simulations of Lennard-Jones spheres, that is, rigid molecules, in a flexible lattice, and therefore could not account for the flexibility of the guest molecules which we have considered here. Indeed, the collisions with the lattice (even fixed) generate a redistribution of the energy between the different vibrational and librational modes and therefore speed up the thermalization. Furthermore, the rather small differences between the transport properties derived from fixed and flexible framework MD simulations of Lennard-Jones spheres in NaA[33] and of flexible methane in silicalite[34] suggested that the thermalization through coupling with the lattice vibrations has little effect on the diffusion. Therefore, it is expected that meaningful conclusions on the self-diffusivities can be drawn from MD simulation with fixed framework. We ensured a good thermalization by performing all simulations within the NVT ensemble, in which a fixed temperature is controlled by a direct scaling of all atomic velocities when the average temperature overcrosses the target temperature by more than 10 K. As pointed out by one of the referees, this method of temperature control is susceptible of changing the dynamical properties of the system, and therefore, the ability of our MD simulations to reproduce accurately the experimental results is questionable. Note, however, that at the present stage of the work our goal is not to compare simulations to experiments but to other simulations: molecular dynamics versus jump diffusion model. In this case, the exact parameters of the simulations are relatively unimportant as compared to the broader trends of the diffusional behavior. However, in further stages of this work our results obtained with direct velocity scaling should be checked against other temperature control methods.

The self-diffusion coefficients were calculated in each case from the mean-square displacement (MSD) of the center of mass (COM) of a sorbed molecule, using Einstein's relationship, and from the velocity autocorrelation function (VACF):[35]

$$D = \lim_{t \to \infty} (1/2it)\langle|\mathbf{r}(t) - \mathbf{r}(0)|^2\rangle \tag{1}$$

$$D = (1/i)\int \langle \mathbf{v}(t)\cdot\mathbf{v}(0)\rangle \, \mathrm{d}t \tag{2}$$

i being equal to 1 for unidimensional, 2 for bidimensional, and 3 for tridimensional diffusion. The two different equations give an indication of the statistical accuracy of the computed self-diffusion coefficient. Practically, D is calculated using eq 1 by a linear fit of the MSD vs time. In eq 2, D is estimated as the mean of the integral of the VACF toward large times. This allows the computation of an accuracy defined as the standard error of the mean of the integral.

The vibrational density of states or power spectrum was computed from the Fourier transform of the VACF. This spectrum shows, in the low frequencies, the external vibrations of the molecular COM and therefore describes the short-time motions of the molecular center of mass.

We also computed the orientational correlation function (OCF), which is defined as:

$$\mathrm{OCF(t)} = \langle \mathbf{e}(\mathrm{t})\cdot\mathbf{e}(0)\rangle \tag{3}$$

where **e** is a unit vector attached to the molecular axis. This

spectrum gives information on the orientational motions and on the librations of the sorbed molecules.

B. Transition Rate Constants. The rate constants were evaluated from the MD runs in the simplest way: given two sites, *i* and *j*, and a boundary hypersurface q_{ij} which defines the transition state (TS), we counted the number of times n_{ij} a molecule crosses the surface. The rate constant are evaluated using the relation:

$$k_{ij} = \lim n_{ij}/t_i \tag{4}$$

where t_i is the total residence time in site *i*. Equation 4 is equivalent to the definition of the rate constants that form the basic assumption of a jump diffusion dynamics:

$$\mathrm{d}n_i/\mathrm{d}t = -k_{i\rightarrow}n_i \tag{5}$$

Indeed, the number of molecules that leaves site *i* to site *j* during *dt* is defined as:

$$\mathrm{d}n_{ij}/\mathrm{d}t = k_{ij}n_i \tag{6}$$

Integrating the last equation over the total duration of the simulation *t* gives

$$n_{ij} = k_{ij}\int_0^t n_i(t)\,\mathrm{d}t \tag{7}$$

where for infinite dilution, $\int_0^t n_i(t)\,\mathrm{d}t$ is simply the total time t_i that the molecule spends in site *i*; for noninfinite dilution, it is the sum of the total time spent by each molecule. Equation 4 has the advantage, over the more usual equation 5, that a rate constant can be defined even when the assumptions of a jump diffusion model cannot be applied.

These equations implies that we can define residence sites for the sorbed molecules and transition states. In fact, this assumption is central to this article, and will be dealt with in more details for each specific case. We have assumed that the sites and transition states can be defined univocally from the COM position in the zeolite channels. This approximation is logical for linear rigid molecules such as *cis*- and *trans*-2-butene but may seem quite crude for 1-butene, which can perform conformational isomerization, or isobutene, which presents also a rotational degree of freedom. We have verified that 1-butene conformational isomerization remains a rapid process in the channels of TON and that no precise conformation is linked to any particular position in the channel. Therefore it is expected that this process can be accounted for by its average effects and that it is unnecessary to include it explicitly.

The exact locations of the TS were evaluated by considering three complementary informations: (i) by a constrained energy minimization along the channel; (ii) by monitoring the positions of the molecular COM during the dynamics; (iii) by counting the number of crossings over a given position during the dynamics. During the constrained minimization, the COM of the guest molecule was set to move freely in a plane perpendicular to the channel axis but constrained in the plane by a quadratic potential of the type $V = a(z - z_0)^2$, where *z* defines the coordinate along the channel axis and *a* was set to ≈2000 kJ/mol to ensure the constraint. Then an energy minimization was performed; the whole molecule was shifted by 0.1 Å, and z_0 was updated to the new position of the COM. This procedure allows to locate the energy minima and the energy barriers in the channel.[32] The plot of the positions of the COM during the dynamics gives the probability that a molecule is at a given position in the channel; obviously, the least probable positions should correspond to the transition states. Similarly the TS, as the least probable region to find the molecular COM, should also be characterized by the smallest number of crossings.

No dynamical correction factor was applied to correct k_{ij}. The dynamical correction accounts for the possible recrossings or multisite jumps. However, we are in a situation where the molecules do not thermalize (as the energy barriers are too small), and therefore where transition state theory (TST) is strictly speaking not applicable. Indeed, we have observed that the dynamical correction factor in these systems shows a continuous decrease to zero and not a plateau characteristic of TST. The dynamical recrossings and multisite jumps are then accounted for directly by the model (by allowing multisite jumps in the Monte Carlo procedure), but the exact rate constant may be difficult to define precisely. Practically, we defined the transition state as a region of size *d*, which was varied in all calculations from 1.0 to 0.05 Å. As *d* decreased, the computed rate constants increased roughly linearly; the limiting value for $d \rightarrow 0$ was used as the input for the jump diffusion model.

C. Monte Carlo Jump Diffusion Model. The residence sites and corresponding rate constants were used as an input for a Monte Carlo jump diffusion model. By simulating the behavior of several molecules in the network of sites assuming uncorrelated jumps, we were able to compute the corresponding MSD from which were derived the self-diffusivities at a given loading.

The simulated system was composed of an integer number of unit cells in each direction *x*, *y*, and *z* and subject to periodic boundary conditions. Each unit cell comprised the required number of sites and connections to represent a unit cell of the original crystal.

There are usually two main possibilities to handle time in a Monte Carlo (MC) simulation:[36] either each step corresponds to a jump and the time interval is defined as the expected residence time in a site[32] or each step corresponds to a time increment, and jumps may or may not occur during this time increment. In the first case, we need multiple time counters (one for each molecule), while in the second case, the time counter is identical with the real time. The second solution was selected as the best possibility to handle multiple molecules in the same system. To avoid the use of a too short time step leading to too long calculations, we had to consider multiple jumps during the same step, which slightly complicated the evaluation of the jump probabilities. The exact calculation of the jump probabilities from the rate constants, and its implementation in an in-house computer code, is described in Appendix A. As each molecule in the system is considered one after the other, the environment of a given molecule does not change while it attempts to jump. This limits the time increment for medium and high loading, which should not be greater than $\Delta t = 2/k_{\max}$, where $k_{\max}$ is the highest transition rate in the system.

To represent some trends of the diffusional behavior of the various butene isomers in zeolite TON and MEL, we implemented a simple model accounting for correlated jumps, by making the assumption that a molecule has a larger probability to jump in the same direction as its previous jump than in the reverse direction. This model is named hereafter CJDM for correlated jump diffusion model. At infinite dilution, the simple mathematical treatment given in Appendix B shows that the diffusional behavior resulting from this assumption is formally identical with a "normal" jump diffusion, where the jump length is divided by the parameter $\sqrt{p_2/p_1}$, p_1 being the probability to jump in the same direction as the previous jump and $p_2 = 1 - p_1$ the probability to jump in the reverse direction. We hence

may define a correlation factor for the jump between sites i and j, $\chi_{ij} = 2p_1^{ij} - 1$, so that

(i) When $0 < \chi_{ij} < 1$, the probability to jump in the same direction is larger than the probability to jump in the reverse direction. Consequently, the jump length is "increased" and the self-diffusivity larger than with no correlation.

(ii) When $\chi_{ij} = 0$, there is no correlation; the process is a normal JDM.

(iii) When $-1 < \chi_{ij} < 0$, the correlation is negative. Consequently, the jump length is "decreased".

The correlation factor is easily computed together with the rate constants from the MD trajectories. The implementation in a computer code is also straightforward. A typical average over 6000 molecules of a 100 ps trajectory took ca. 30 s on an IBM RS/6000 Model 340 workstation.

3. Results and Discussion

A. Zeolite TON. Zeolite TON[19] is interesting as a model material for this study. Indeed, it presents unidirectional 4.4 × 5.5 Å elliptic channels along [001], with a very smooth energy surface. Diffusion of butene isomers is therefore quite simple to represent at infinite dilution; however at high loading, these systems present single-file diffusion, as was evidenced experimentally for CH_4, CF_4, and CO_2 in $AlPO_4$-5 and theta-1.[37−39] In addition to this relative simplicity, zeolite TON has been previously studied as a potential catalyst for butene skeletal isomerization.[24] Furthermore, we have shown that, unlike some other channel zeolites (MEL, MFI, FER, MTT, HEU), TON seems to favor the diffusion of isobutene as compared to *trans*-2-butene, which in these other zeolites is diffusing faster than all other butene isomers.[32]

Molecular Dynamics. The simulation cell consisted of 2 × 1 × 4 unit cells of zeolite TON, building a 28.3 × 17.9 × 21.0 Å block containing four identical and independent channels. In the channels were placed initially four butene molecules (two in the same channel and two in different channels) so that a single MD run could give simultaneously the self-diffusivity both at infinite dilution and at a loading of 0.5 molecule/uc channel. Four independent 148 ps runs were performed to give a better statistical average. While the MD runs at infinite dilution are intended to provide "physical" results, it should be stressed that the runs performed with 0.5 molecule/uc channel give "unphysical" results which we can compare to a JDM approach but not to experiment. Indeed, the diffusional behavior of a single-file system is very different if one considers periodic boundary conditions (PBC) or limiting or reflecting boundaries.[41] Obviously the small system used here cannot reproduce the physical behavior of molecules which are not subject to PBC. MD studies of single-file systems indeed require thousands of atoms.[37,43] However, it is our hope that the trends observed at short time on the diffusion with 0.5 molecule/uc channel can be extended, on the basis of a JDM approach, to a more realistic modeling of the system.

Table 1 presents the self-diffusivities computed from the MD trajectories at infinite dilution and for 0.5 molecule/uc channel. Note a certain difference between the self-diffusion coefficient from NVT MD trajectories presented here and from NVE trajectories published elsewhere with the same force field and model.[32] The previous NVE results suffered from a rather high statistical unaccuracy (higher than the accuracy obtained here as the averages were performed on fewer molecules). Furthermore, the temperature control in NVE simulations with fixed framework is rather poor, which resulted here in lower "effective temperature" for the motion of the COM in the case of NVE as compared with NVT. However, the trends observed in NVE simulations are still present in the NVT ones. While in most other channel type zeolites rather high differences can be observed between the self-diffusivities of the different isomers,[32] in TON they roughly have the same order of magnitude. In particular, while in the other channel zeolites diffusion of isobutene is strongly hindered, which results in self-diffusivities up to 20 times lower than that of *trans*-2-butene in MTT, it is seen here that diffusion of isobutene is favored over *trans*-2-butene. Reasons for this will be analyzed later in more details.

TABLE 1: Self-Diffusion Coefficients D in 10^{-8} m^2/s, Rate Constants k_{ij} in ps^{-1}, and Correlation Factors χ_{ij} for the Butene Isomers in Zeolite TON at 623 K, Determined from Simulations Performed with the cff91_zeo Force Field of Biosym/MSI

	trans-2-butene		*cis*-2-butene		1-butene		isobutene	
	a	*b*	*a*	*b*	*a*	*b*	*a*	*b*
D(MSD)	6.0	1.0	5.4	1.9	3.0	2.7	6.2	2.7
D(VACF)	5.9	1.4	5.1	1.8	3.2	3.5	7.4	2.1
D(CJDM)	3.6	1.2	5.2	1.8	5.0	1.7	6.6	2.6
k_{12}	0.42	0.37	0.64	0.54	0.50	0.47	0.49	0.52
k_{21}	0.42	0.37	0.61	0.68	0.58	0.57	0.53	0.54
χ_{12}	0.09	−0.12	0.14	−0.09	0.14	−0.13	0.31	−0.04
χ_{21}	0.09	−0.12	0.09	−0.04	0.16	−0.04	0.28	−0.04
TS_{12}	1.1		1.0		1.0		0.0	
TS_{21}	3.7		3.8		3.8		2.5	
E_{12}	3.6		1.2		4.1		2.7	
E_{21}	3.7		2.1		4.0		1.8	

[a] Infinite dilution. [b] Loading of 0.5 molecule/uc channel. D(MSD) is computed from a linear fit of the mean-square displacement of the COM with time; D(VACF) is computed from the velocity autocorrelation function; D(CJDM) is computed from a model of correlated jump diffusion, taking as input the rate constants k_{ij} and correlation factors χ_{ij} computed from the MD trajectories. TS_{ij} is the position of the transition state in the channel in Å, evaluated from the MD trajectories and from a constrained energy minimization along the channel; E_{ij} is the corresponding energy barrier, in kJ/mol.

At 0.5 molecule/uc channel, the diffusivities are lower than at infinite dilution, with the notable exception of 1-butene. However, there is a very large difference in the decrease of the diffusivities between the isomers: to a decrease for *cis*-2-butene and isobutene rather consistent with what is expected from theory, assuming there is no strong guest−guest interactions, corresponds a dramatic decrease for *trans*-2-butene and no change for 1-butene. Therefore, we see that the difference between the diffusion of the various butene isomers in TON is larger at finite loading than at infinite dilution. Even if these "unphysical" self-diffusivities serve only as indications of the probable trends of the real system, they illustrate the influence of the guest intermolecular interactions. Rather interestingly, the specificity of TON to favor diffusion of isobutene over *trans*-2-butene is conserved and even enhanced in the simulations at 0.5 molecule/uc channel.

Figure 1 presents the low-frequency vibrational density of states (DOS) computed from the velocity autocorrelation functions, for each isomer, at infinite dilution and 0.5 molecule/uc channel. Their shape can be easily separated in three components corresponding to the three directions x and y, perpendicular to the channel axis, and z, parallel to the channel axis. The well-defined peaks along x and y represent the rattling motions perpendicular to the elliptic channel of TON. There is no difference at all between the DOS along x and y when the loading is decreased, which was expected considering the single-file character of the system. The two separated components observed for linear butenes arise from the ellipticity of the channels of TON, while the conformation adopted by isobutene in the channel merges the two peaks along x and y together

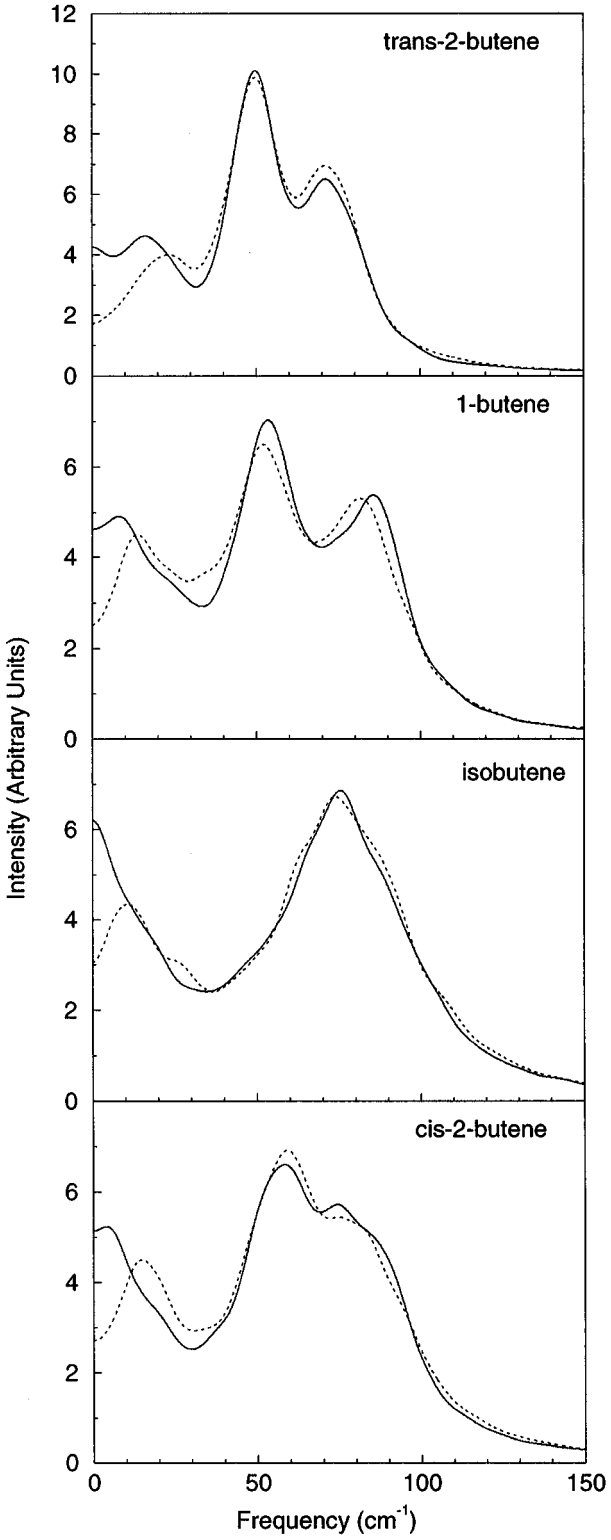

Figure 1. Vibrational density of states of the butene isomers in zeolite TON, at infinite dilution (solid lines) and loading of 0.5 molecule/uc channel (dotted lines), computed from the average over eight 148 ps MD trajectories at 623 K, performed with the cff91_czeo forcefield of Biosym/MSI.

(Figure 1). Diffusion along the channel axis is characterized by a low-frequency peak ($\approx$10 cm^{-1}) continued by a tail toward 0 cm^{-1}, markedly lower for higher loading than for infinite dilution; note that this peak fades at higher loading even for 1-butene where diffusion is not significantly lower. There is a slight shift of this diffusion peak at higher loading, which characterizes the interactions between two guest molecules. In all cases, this shift remains very weak, indicating that no

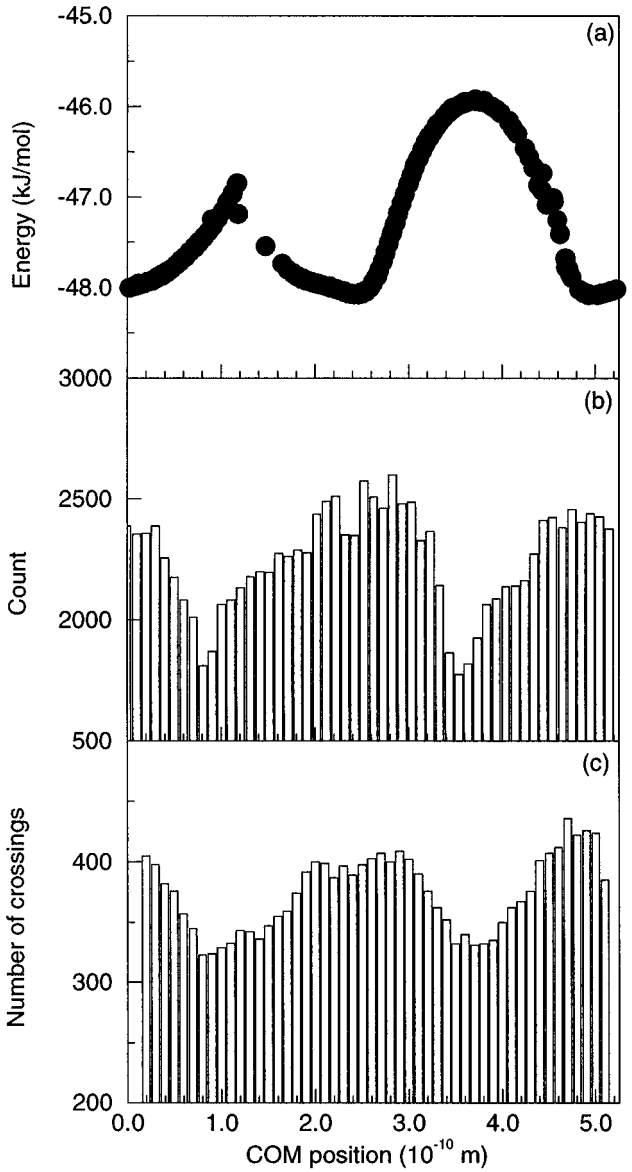

Figure 2. Behavior of *cis*-2-butene in zeolite TON simulated using the cff91_czeo forcefield of Biosym/MSI. (a) Minimum energy path computed from a constrained dynamics along the channel axis. (b) Probability to find the COM at a given position in the channel during the 148 ps MD run at 623 K. (c) Number of crossings of the COM over a virtual barrier placed at a given position in the channel, computed from the same 148 ps MD run.

supermolecular complex is created from the two individual molecules. Therefore the interactions, which cause the high difference between the diffusion of the butene isomers at 0.5 molecule/uc channel, remain weak.

Jump Diffusion Model. As stated in section 2B, an analysis of the MD trajectories as a jump diffusion process demands that we can define precise sites in the channels, separated by transition states. The sites and location of the TS were defined from a constrained energy minimization along the channel, a plot of the most probable positions of the COM during the MD run, and a record of the number of crossings from one side of the TS to the other during the MD run. The corresponding graphs, for the example of *cis*-2-butene in zeolite TON at infinite dilution, are presented in Figure 2. Clearly two different energy minima are found in the 5.25 Å channel, separated by energy barriers located at ca. 1.0 and 3.8 Å. These energy barriers correspond exactly to the least probable position of the COM and also to the lowest number of crossings. Therefore, the

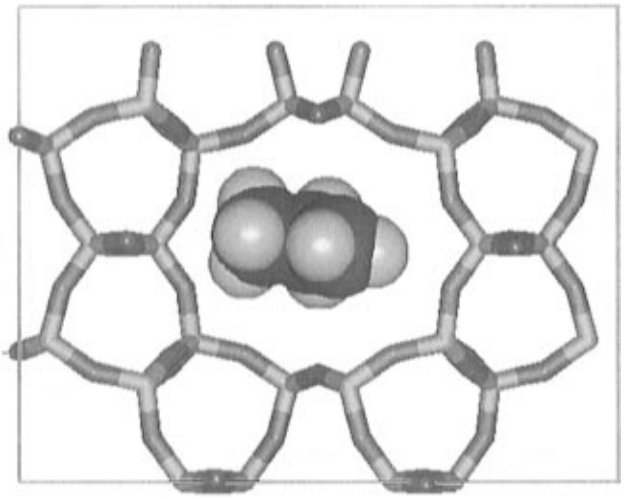

Figure 3. View on the minimum energy position of isobutene in TON, computed by a constrained dynamics along the [001] channel axis, using the cff91_czeo forcefield of Biosym/MSI.

position of the TS can be univocally positioned at 1.0 and 3.8 Å for *cis*-2-butene in TON. Similar graphs were computed for the other butene isomers. Although the energy barrier positions are less well defined for 1-butene and isobutene, in conjunction with the plot of the COM positions and number of crossings, we could precisely define the position of the TS. Two sites are found for each isomer. We have verified on the MD trajectories that each site can accommodate only one molecule. The positions of the TS and the height of the corresponding energy barriers are given in Table 1. Note that the TS positions are sensibly the same for all linear butenes but different for isobutene, due to its different global shape. There is a good correlation between the energy barriers and the computed diffusivities at infinite dilution. This suggests that an Arrhenius form of the jumping rate constant might be applicable here. This correlation was expected: indeed, the diffusivities depend on the free energy barrier to the diffusion along the channel (which we did not compute). As the channel surface is rather smooth, there is probably only a very small change in the entropy of the sorbed molecule, so that the free energy profile is likely to follow the minimum energy path. Therefore, the high self-diffusivity of *cis*-2-butene and isobutene is linked to the small energy barriers (from 1.2 to 2.7 kJ/mol). This is probably due to the complementarity between the shape of the molecule and that of the elliptical pore. Indeed, the plate-shaped isobutene (Figure 3) and the compact shape of *cis*-2-butene fit much better in the channel than the linear *trans*-2-butene. The higher diffusivities of isobutene and *cis*-2-butene then agree with the concept of "floating molecules" of Derouane and co-workers.[44,45]

From the TS positions and MD trajectories, we have determined the jumping rate constants at infinite dilution. However, the introduction of these rate constants in the MC JDM approach described in Section 2C leads in all cases to much lower diffusivities than the ones directly computed from the MD trajectories. This shows that a direct JDM is *not* applicable for butene isomers in the channels of TON at 623 K. Indeed, the assumption of uncorrelated jumps, central to the "normal" JDM, does not hold in these systems. Therefore, we have used the JDM approach modified to account for correlated jumps as described in Section 2C. Table 1 presents the rate constants and correlation factors computed from the 148 ps MD trajectories at 623 K for the four butene isomers in TON, while Figure 4 presents graphically the comparison between the MSD values, computed directly from the MD

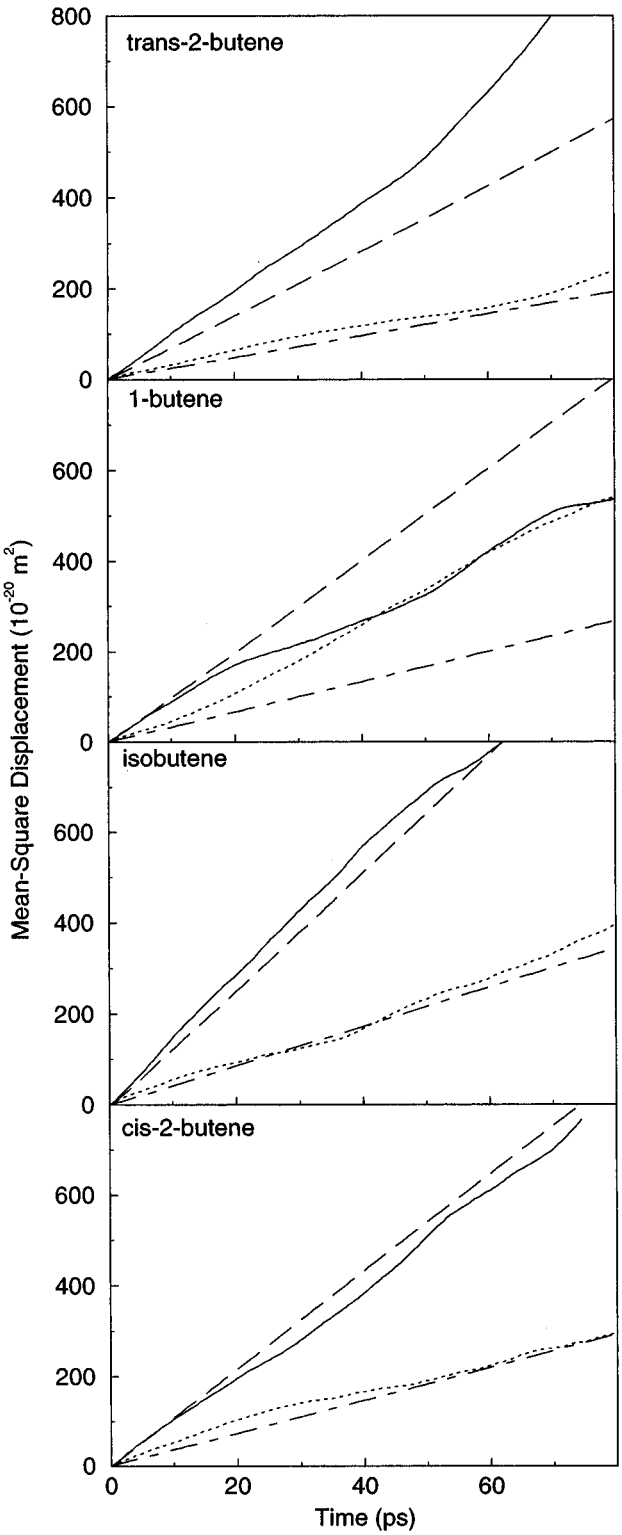

Figure 4. Mean-square displacement of the butene isomers in zeolite TON, computed using the cff91_czeo force field of Biosym/MSI. Solid lines: from an average over eight 148 ps MD trajectories at 623 K, at infinite dilution. Dotted lines: from the same MD runs at a loading of 0.5 molecule/uc channel. Long dashed lines: from a two-sites CJDM at infinite dilution, using the transition probabilities computed from the MD runs at infinite dilution (cf. Table 1). Dot−dashed lines: from a two-sites JDM at a loading of 0.5 molecule/uc channel, using the same rate constants as for infinite dilution.

trajectories and from the CJDM, both at infinite dilution and at 0.5 molecule/uc channel. In the latter case, we incorporated only two unit cells in the CJDM so that the results could be directly compared with the MD trajectories. The rate constants

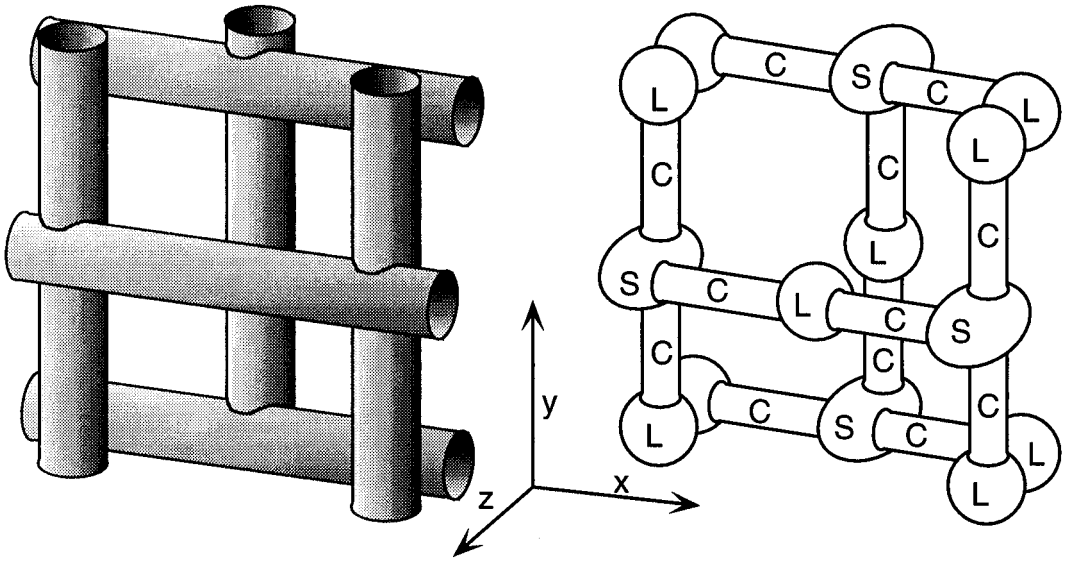

Figure 5. Sketch (left) of the channel system of zeolite MEL and (right) of the corresponding network of three sites (S), (L), and (C) used in the three-sites JDM calculation; in the case of the two-sites JDM, only sites (S) and (L) were considered.

TABLE 2: Self-Diffusion Coefficients D in 10^{-8} m^2/s for the Butene Isomers in Zeolite MEL at 623 K and Infinite Dilution, Determined from Simulations Performed with the Cff91_zeo Force Field of Biosym/MSI[a]

	trans-2-butene			*cis*-2-butene			1-butene			isobutene		
	D	D_{xy}	D_z	D	D_{xy}	D_z	D	D_{xy}	D_z	D	D_{xy}	D_z
D(MSD)	2.2	3.0	0.43	2.5	3.4	0.55	4.5	6.6	0.31	1.1	1.5	0.34
D(VACF)	2.1			2.5			4.8			1.8		
D(two-sites JDM)	2.3	3.2	0.52	3.2	4.5	0.57	3.2	4.5	0.70	2.9	4.1	0.59
D(three-sites JDM)	1.4	1.9	0.37	1.7	2.4	0.37	1.7	2.3	0.40	1.4	1.9	0.35
D(three-sites CJDM)	2.2	3.1	0.53	2.8	4.0	0.50	3.8	5.3	0.75			

[a] D(MSD) is computed from a linear least-squares fit of the mean-square displacement of the COM of butene isomers during the 200 ps MD run; D(VACF) is computed from the velocity autocorrelation function; D(n-sites JDM) is computed from a jump diffusion model with n sites, taking as input the rate constants computed from the MD trajectories. D(three-sites CJDM) is computed from a three-sites correlated jump diffusion model with the same rate constants as for the three-sites JDM.

used as input for a loading of 0.5 molecule/uc channel are the ones computed at infinite dilution. Although results of the CJDM are in much better agreement with the MD ones than for the simple JDM, there is a marked discrepancy. In particular, the difference is large even at infinite dilution for *trans*-2-butene and 1-butene. This shows that the process for these two molecules is basically *not* a correlated jump diffusion. On the other hand, the rather good agreement for isobutene and *cis*-2-butene suggests that the CJDM is a good approximation of the diffusional behavior for these two molecules. This illustrates a basic difference in the diffusion process between the butene isomers. The correlation appears to be rather small for all linear butenes (<0.16) but much higher for isobutene (0.31); this is consistent with the smaller energy barrier to the diffusion calculated for the latter isomer. However, as the correlation factor for *cis*-2-butene is very small despite lower energy barrier, we see that there is no direct link between the two quantities.

B. Zeolite MEL. Zeolite type MEL[19] also represents a good model material for our investigations: indeed, its 3-D channel system is made up of only one type of nearly cylindrical straight 5.3×5.4 Å channels running along [100] and [010]. However, there are two types of intersections between these channels: small intersections, which build cavities of about 1.5 times the size of the channel; and large intersections, which are more alike short channels along [001], as the distance between the center of the intersecting channels amounts to $\approx$5 Å. MEL is basically made up of three distinct sites in which the surroundings of the guest molecules is different: channels (C), small intersections (S), and large intersections (L). A sketch of the channel systems, and of the corresponding sites, is depicted in Figure 5. Such system slightly complicates the analysis of the MD trajectories by comparison to TON, as we have to consider these three different sites to draw any meaningful conclusion from the vibrational density of states. In a first part, we have analyzed the MD trajectories of the four butene isomers in MEL at infinite dilution, both directly and with a JDM; in a second part, we have investigated their diffusional behavior versus increasing loading. In all cases, the simulation cell was made up of two unit cells of MEL along [001], building an approximately $20.5 \times 20.5 \times 27.5$ Å block, in which we investigated the self-diffusion of 1−20 molecules. Due to computer time limitations, the duration of the run varied from 200 ps for 1 molecule to 60 ps for 20 molecules. The results were averaged over five and two independent runs, in the case of one molecule and five molecules, respectively, to get a better statistical average.

Infinite Dilution. Table 2 presents the diffusion coefficients computed at infinite dilution from the VACF and the MSD. We separated the diffusion of the guest molecules into two distinct components: along x and y, that is, in the plane of the channels, and along z, that is, perpendicular to the plane of the channels. The 2-D coefficient computed in the channel plane is twice the coefficient along a channel. As expected, the diffusion coefficient perpendicular to the plane is much smaller than that in the plane, due to the tortuosity of the path along [001]. However, the diffusion coefficient of all isomers is of the same order of magnitude, both parallel and perpendicular to the channel plane. As for TON, let us note a large discrepancy, both in absolute and relative values, with the self-

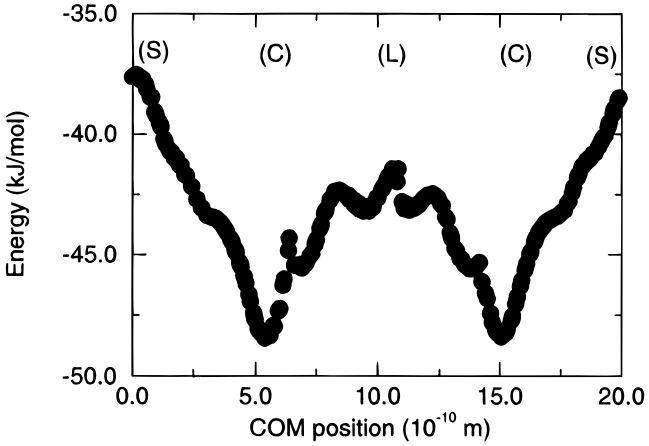

Figure 6. Minimum energy path of *cis*-2-butene in zeolite MEL, computed from a constrained dynamics along the [100] channel axis, using the cff91_czeo force field of Biosym/MSI.

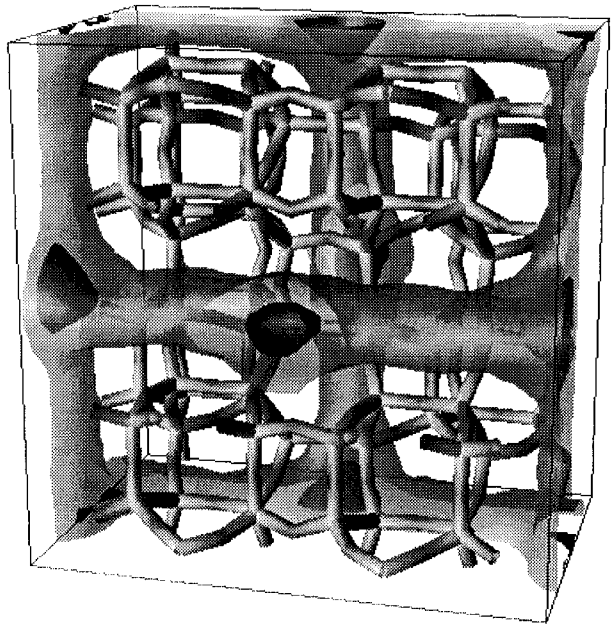

Figure 7. 3-D plot of the probability to find the COM of *cis*-2-butene at a given position in zeolite MEL at infinite dilution and 623 K, computed from the average over five 200 ps MD trajectories, using the cff91_czeo force field of Biosym/MSI. Light shaded shape: probability density 2×10^{-5}. Dark shaded shape: probability density 6×10^{-4}. Plot depicted with IBM DataExplorer.[46]

diffusion coefficients computed earlier in the NVE ensemble.[32] Beside the rather high statistical inaccuracy of the latter values, a direct comparison is not possible as the latter data were computed with five molecules. However, some similar trends are found, as isobutene diffuses slower than the linear isomers.

It was found in our previous study[32] that the channel sites (C) correspond to the minimum energy positions for all butene isomers. This is confirmed by a constrained minimization along the channel, which shows that both channel intersections are positions of maximum energy, with energy barriers ranging from 8 to 10 kJ/mol. The minimum energy path along the [100] channel is given in Figure 6 for the example of *cis*-2-butene. However, a 3-D plot of the most probable positions of the COM of butene isomers at infinite dilution shows that there is a much larger probability to find the COM at the intersections than inside the channels (Figure 7). This indicates, in contrast to what was found in TON, that there are large entropy effects which influence the self-diffusion. Indeed, the diffusion is governed by the free energy of the molecule along its path. We

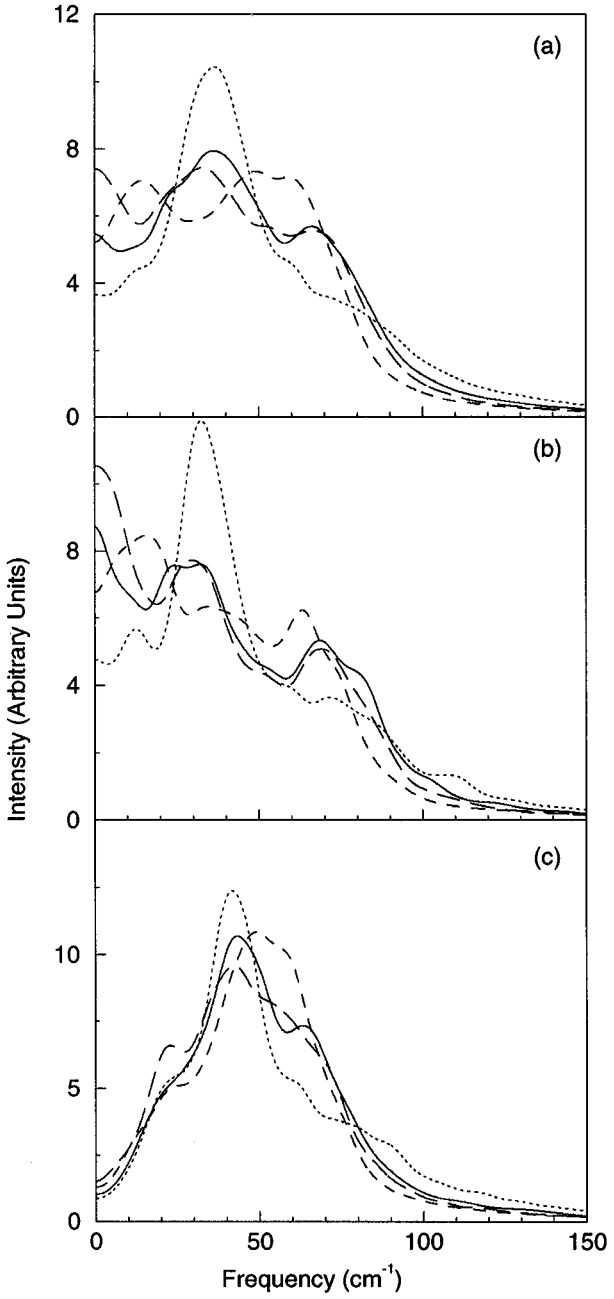

Figure 8. Vibrational density of states of the butene isomers in zeolite MEL at infinite dilution and 623 K, computed from the average over five 200 ps MD trajectories using the cff91_czeo force field of Biosym/MSI. Solid lines: *cis*-2-butene. Dotted lines: isobutene. Dashed lines: *trans*-2-butene. Long dashed lines: 1-butene. (a) Along all three axes. (b) Along *x* and *y*. (c) Along *z*.

have estimated the entropy barrier $T \times S$ of *cis*-2-butene between sites (S) and (C) from the external vibrational frequencies and the possibility of some rotational freedom in the cavities and showed that it could amount up to 25 kJ/mol at 623 K, that is, more than twice the energy barrier, thus inversing the minimum free energy position as compared to 0 K.

Figure 8a−c presents the vibrational density of states (DOS) of the butene isomers in MEL, in all directions, in the plane of the channel (*x* and *y*) and perpendicular to the channel plane (*z*), respectively. The DOS in the channel plane includes all vibrations along the channel axis but also the vibrations perpendicular to the channel axis but in the same plane. Indeed, it is not possible to separate the contributions along and perpendicular to the channels in the intersections. Due to the existence of three distinct sites, these DOS present a rather

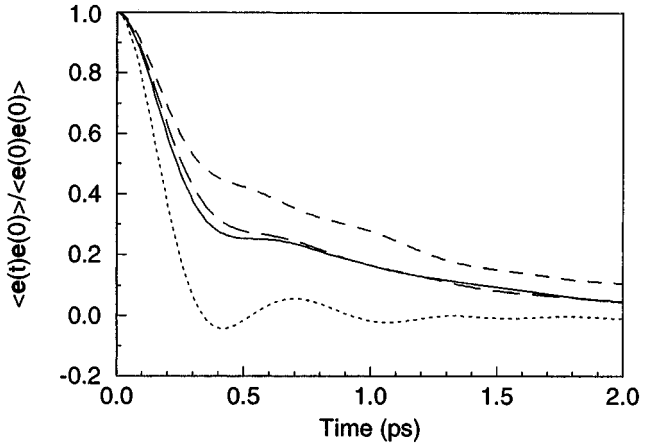

Figure 9. Orientational correlation function of the butene isomers in zeolite MEL at infinite dilution and 623 K, computed from the average over five 200 ps MD trajectories using the cff91_czeo force field of Biosym/MSI. Solid lines: *cis*-2-butene. Dotted lines: isobutene. Dashed lines: *trans*-2-butene. Long dashed lines: 1-butene.

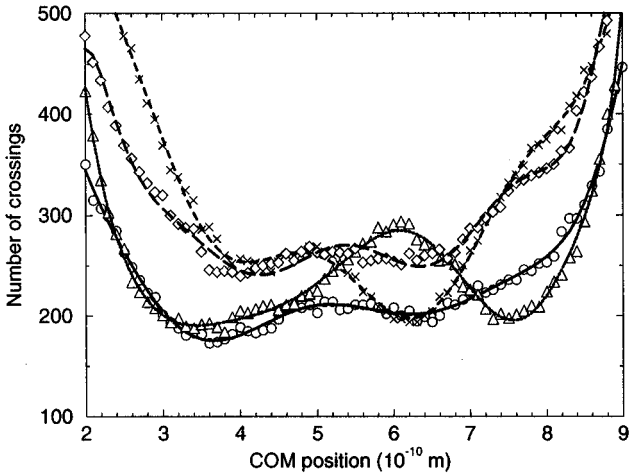

Figure 10. Number of crossings over a given virtual barrier of the butene isomers in zeolite MEL, computed from five 200 ps MD simulations at infinite dilution and 623 K, using the cff91_czeo force field of Biosym/MSI. Symbols are number of crossings from the MD runs, lines are a tenth degree least-squares fit of the points and serve as guidelines for the eyes. Circles, solid line: *cis*-2-butene. Triangles, dotted line: isobutene. Crosses, dashed line: *trans*-2-butene. Squares, long dashed line: 1-butene.

complicated shape. However, both the spectra in the channel plane and perpendicular to it appear to be made of three main peaks at lower (LF), medium (MF), and higher (HF) frequency. We may separate the contribution in each site by computing the Fourier transform of $\langle \mathbf{v}(t)\Theta_i(t)\cdot\mathbf{v}(0)\Theta_i(0)\rangle$, where $\Theta_i(t)$ is a function equal to 1 if the molecule is in site i and 0 otherwise. The resulting observations are reported hereafter:

(i) The LF peak in the channel plane ($\approx$10−15) originates from the molecules located in sites (C) and (L) and is characteristic of diffusive motions.

(ii) The MF peak in the channel plane ($\approx$30−40) originates from the molecules located in sites (S) and can be attributed to the rattling motions inside the large cavities.

(iii) The HF peak in the channel plane ($\approx$60−80) originates from the molecules located in sites (C) and (L) and corresponds to the rattling motions perpendicular to the channel axis.

(iv) The LF peak along z appears around 25 only from the DOS computed in sites (L) and corresponds to the "diffusion" in the short channels formed at the large intersections.

(v) The MF peak ($\approx$50) is found only from the DOS in sites (S), while a peak at slightly higher frequency ($\approx$60) appears from the DOS at sites (C); they both characterize the rattling motions perpendicular to the channel plane, in sites (S) and (C), respectively.

In all cases, the MF peak is the largest, indicating that the guest molecules spend more time in the sites (S); this agrees with the graphical display of Figure 7. The diffusion peak, both in the channel plane and perpendicular, also agrees with the self-diffusion coefficients. This shows that the long-time diffusion computed from the MSD is directly connected to the short-time diffusion behavior evidenced by the DOS. Since the same peaks appears for all molecules at similar frequencies (taking into account the different size of each molecule), the short-time motions of all butene isomers in the channels of MEL are comparable.

Figure 9 presents the orientational correlation function (OCF) of the butene isomers in MEL. In all cases, there is a very quick loss of the orientation in less than 2.0 ps, through the collisions with the zeolite walls. For isobutene, we observe a remnant of rotational motion with a period of $\approx$0.8 ps, which of course is more hindered for linear butenes. This residual rotational mobility has a major influence on the diffusivity of butene isomers: indeed, the entropy barrier to the diffusion mainly originates in the hindering of the rotational degrees of freedom between the intersections and the channels; as the hindering is less pronounced for isobutene, the resulting free energy profile is likely to follow more closely the minimum energy path than for linear butenes.

The definition of the position of the transition states can be obtained by plotting the number of crossings over a given barrier along the 20.5 Å channel of MEL (Figure 10). As the channels are symmetrical, we investigated only the position from 2 to 9 Å. Positions between 0 and 2 Å and between 9 and 10.25 Å correspond to the channel intersections and therefore the number of crossings in only one direction has no meaning in these regions. The exact position of the TS in the channel is rather poorly defined. In particular, there does not seem to be any well-defined channel site (C) for the linear butenes as there is only one marked TS. In the case of isobutene, the existence of two precise TSs probably comes from the lower entropy barrier, as discussed in the preceding paragraph. Therefore, it is not conclusively evident whether the system should be modeled by two different sites (S) and (L) only, or by three sites. Hence, we used both approaches to represent the diffusion. The positions of the TS and the corresponding rate constants are given in Table 3. Along the [001] axis, a TS can be found in the middle of the large intersections, while there is no evidence of any such transition state in the small intersections. Consequently, the sites (L) have been divided into two different sites along [001], between which we can compute a transition probability. The total network of sites, and the connections, are illustrated in Figure 5. The self-diffusivities computed from the JDM are compared to the same values computed from the MD simulation in Table 2 and in Figure 11. We see that a two-sites JDM fits very well the behavior of the linear butenes while a three-sites JDM underestimates dramatically the self-diffusion coefficient. On the contrary, a three-sites JDM is well adapted to isobutene but not a two-sites JDM. In the case of linear butenes, a three-sites CJDM can fit the MSDs if we assume correlated jumps along the channels. A computation of the correlation factor from the MD runs resulted in a poor average, due to the high number of different correlated jumps to consider: (S) → (C) → (L), (S) → (C) → (S), etc. Consequently, we used a mean correlation factor for all jumps along a channel, fitted to reproduce the observed MSD; they are listed in Table 3.

TABLE 3: Position of the Transition States (TS) in Å Estimated from a Plot of the Number of Crossings over a Virtual Barrier in the Channel of MEL (Figure 10), and Transition Probabilities k_{ij} in ps^{-1} between the Sites (S) and (L) (2-Sites JDM) and (S), (C), and (L) (3-Sites JDM), Computed from Five 200 ps MD Runs at Infinite Dilution and 623 K with the Cff91_czeo Force Field of Biosym/MSI[a]

	trans-2-butene	*cis*-2-butene	1-butene	isobutene
TS	6.2	3.7	3.8	7.5
$4k_{SL}$	0.107	0.186	0.167	0.118
$2k_{LS}$	0.149	0.161	0.165	0.228
k_{LL}	0.20	0.10	0.19	0.24
TS1	4.3	3.7	3.8	3.4
TS2	6.2	6.4	5.9	7.5
$4k_{SC}$	0.174	0.183	0.167	0.146
k_{CS}	1.26	0.79	1.17	0.41
k_{CL}	0.90	0.73	1.22	0.40
$2k_{LC}$	0.150	0.243	0.196	0.230
k_{LL}	0.20	0.12	0.21	0.24
χ	0.48	0.48	0.85	0.0

[a] The correlation factor χ for the jumps between sites (S), (C), and (L) aligned in the same channel was estimated by a linear fit of the resulting mean-square displacement of the COM with the MSD computed from the MD trajectories. $4k_{S\alpha}$ and $2k_{L\alpha}$ represent the total probability to get out of the sites (S) and (L), respectively.

The fit with three sites for isobutene at infinite dilution but only two sites for linear butenes illustrates a major difference in the diffusion behavior of the branched as compared to the linear isomers. Indeed, as the rate constants for the diffusion are rather similar for all isomers, the reason isobutene diffuses slower than linear butenes in MEL at 623 K appears to be that isobutene thermalizes in the channel sites (C). Moreover, it seems that this is due not to larger energy barriers to the diffusion but rather to its rest of rotational mobility in the large channels of MEL. The absence of thermalization for linear butenes explains the very large transition probability to get out of a channel site (C) (that is, k_{CS} and k_{CL}), as compared to the probability to get in a site (C) (that is, k_{SC} and k_{LC}). Evidently, this corroborates the preceding analyses, where we have found that the molecules spend much more time at the intersections than in the channels.

As a general rule, a jump diffusion model (JDM) appears to reproduce very well the diffusion behavior of all butene isomers in zeolite MEL at infinite dilution, either by a two- or three-sites JDM. As the self-diffusion coefficients both in and perpendicular to the channel plane are well fitted, this shows that the network of sites presented in Figure 5 is well chosen. The correlated jump diffusion model used for linear butenes also matches the self-diffusivities computed from the MD runs, both in and perpendicular to the channel plane; but the fitted correlation factor introduces an external bias, and therefore this approach has still to be confronted with the diffusion behavior observed at nonzero loading.

Nonzero Loading. The self-diffusion of the different butene isomers in MEL was investigated with 5, 10, 15, and 20 molecules in the simulation cell, which correspond to a coverage of 2.5, 5, 7.5, and 10 molecules/uc, respectively. Figure 12 presents the density of probability to find the COM of a *cis*-2-butene molecule in the zeolite channels, for a coverage of 10 molecules/uc. The same isosurface values as for Figure 7 were used for the graphical display. The contrast with Figure 7 is striking: while at infinite dilution, the molecules are mostly to be found at the intersections, for 10 molecules/uc, there is a larger probability to find the molecules in the channels. Hence, after the intersections are occupied, the guest molecules pack within the channels. This is corroborated by the evolution of the DOS (Figure 13): the middle frequency peaks (MF) corresponding to vibrations in sites (S) fades while the high-frequency peaks attributed to the vibration in the channel sites (C) becomes stronger. This evolution is accompanied by a decrease of the diffusion tail as the diffusion becomes more and more blocked. Note that for *trans*-2-butene at 2.5 molecules/uc, the diffusion tail is larger than at infinite dilution. Therefore,

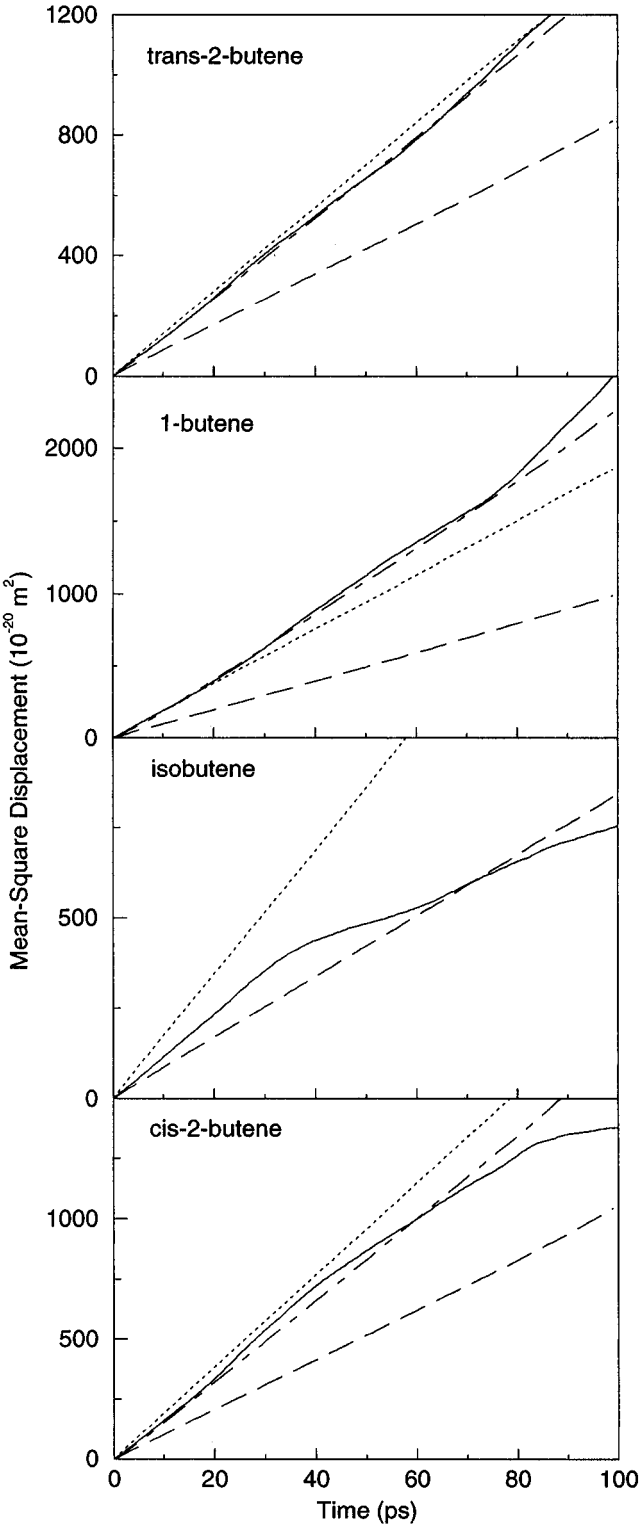

Figure 11. Mean-square displacement of the butene isomers in zeolite MEL. Solid lines: from an average over five 200 ps MD trajectories at 623 K, with the cff91_czeo force field of Biosym/MSI, at infinite dilution. Dotted lines: from a two-sites jump diffusion model, using the rate constants computed from the MD trajectories at infinite dilution. Long dashed lines: from a three-sites JDM. Dot dashed lines: from a three-sites JDM with correlation.

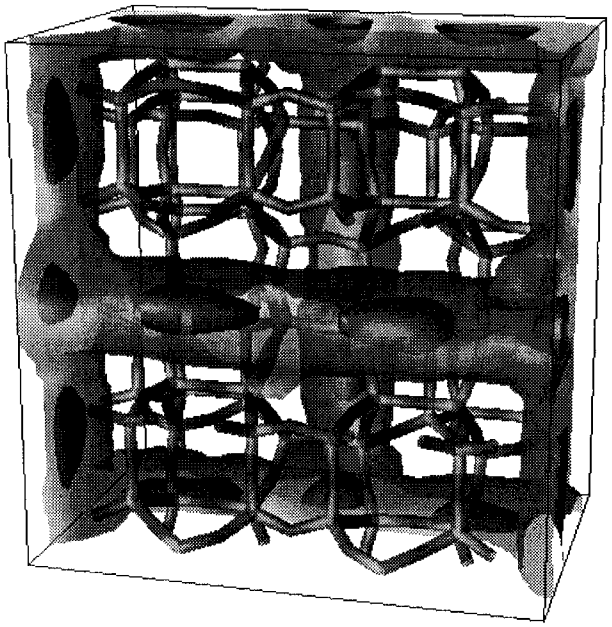

Figure 12. 3-D plot of the probability to find the center of mass of *cis*-2-butene at a given position in zeolite MEL at a loading of 10 molecules/uc and 623 K, computed from a 60 ps MD trajectory with 20 molecules, using the cff91_czeo force field of Biosym/MSI. Light shaded shape: probability density 2×10^{-5}. Dark shaded shape: probability density 6×10^{-4}. Plot depicted with IBM DataExplorer.[46]

the short-time diffusive motions seem to be enhanced for this coverage. This could be due to cooperative motions of the *trans*-2-butene molecules in the channels of MEL; however, there is no other evidence of such behavior neither in the DOS nor in the distribution of the distances between the molecules.

Careful examination of the DOS in each direction shows that the evolution of the shape of the peaks as a function of the coverage, which seems roughly continuous in Figure 13 in fact happens in two distinct steps. First, up to 10 molecules, there is a decrease of the MF peak along [001] (corresponding to the vibration along *z* in the small intersections) as well as of the diffusion tail, while there is no major change in the other peaks, which shows that the initial additional molecules mainly occupy these intersections. Then, the decrease of the MF peak in the channel plane (corresponding to the parallel motions in the small intersections) and of the LF peak along [001] (corresponding to the vibration inside the large intersections) shows that the large intersections and the channels become more populated. The initial increase of the population in the sites (S) is in accordance with the rate constants computed at infinite dilution, which favor these particular sites.

The evolution of the orientational correlation function, presented in Figure 14, is very similar for all linear butenes: the orientational mobility decreases dramatically as the loading increases, so that more than half of the molecules keep their original orientation over more than 30 ps at 10 molecules/uc. Some slight oscillations remain at high loading and correspond to the rotation of these linear molecules around their molecular axis. This rotation of course completely disappears for isobutene. However, the larger orientational mobility of this isomer is evidenced by the complete fading of the orientational correlation function in less than 3 ps.

Both a two-sites JDM and a three-sites CJDM were used to compute the self-diffusivities of linear butenes in MEL, using as input the rate constants computed at infinite dilution and listed in Table 3; in the case of isobutene, only the three-sites JDM approach was applied, as it was shown to lead to a good fit of the MSD at infinite dilution. As the loading increases, it is

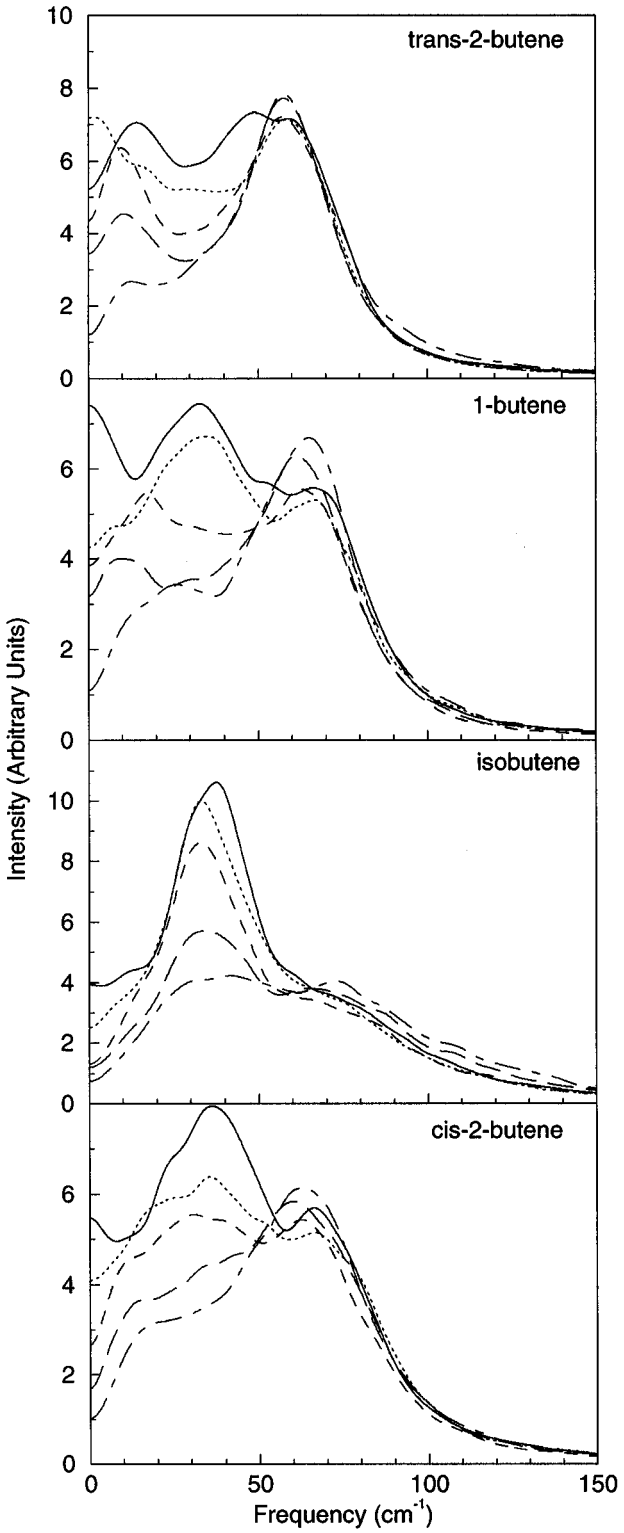

Figure 13. Vibrational density of states of the butene isomers in zeolite MEL, computed from MD trajectories at 623 K using the cff91_czeo force field of Biosym/MSI. Solid lines: zero loading. Dotted lines: 2.5 molecules/uc. Dashed lines: 5 molecules/uc. Long dashed lines: 7.5 molecules/uc. Dot dashed lines: 10 molecules/uc.

necessary in some cases to consider the possibility for more than one molecule to occupy the same site. Of course the rate constant will be different if the site is empty or already occupied; however, it is not possible to compute these rate constants from the MD trajectories at zero loading, so that they have to be evaluated from the MD results at higher coverage. To simplify the procedure, we assumed that the transition probability $k_{ij}(n)$ to jump from a site *i* to a site *j* already occupied by *n* molecules

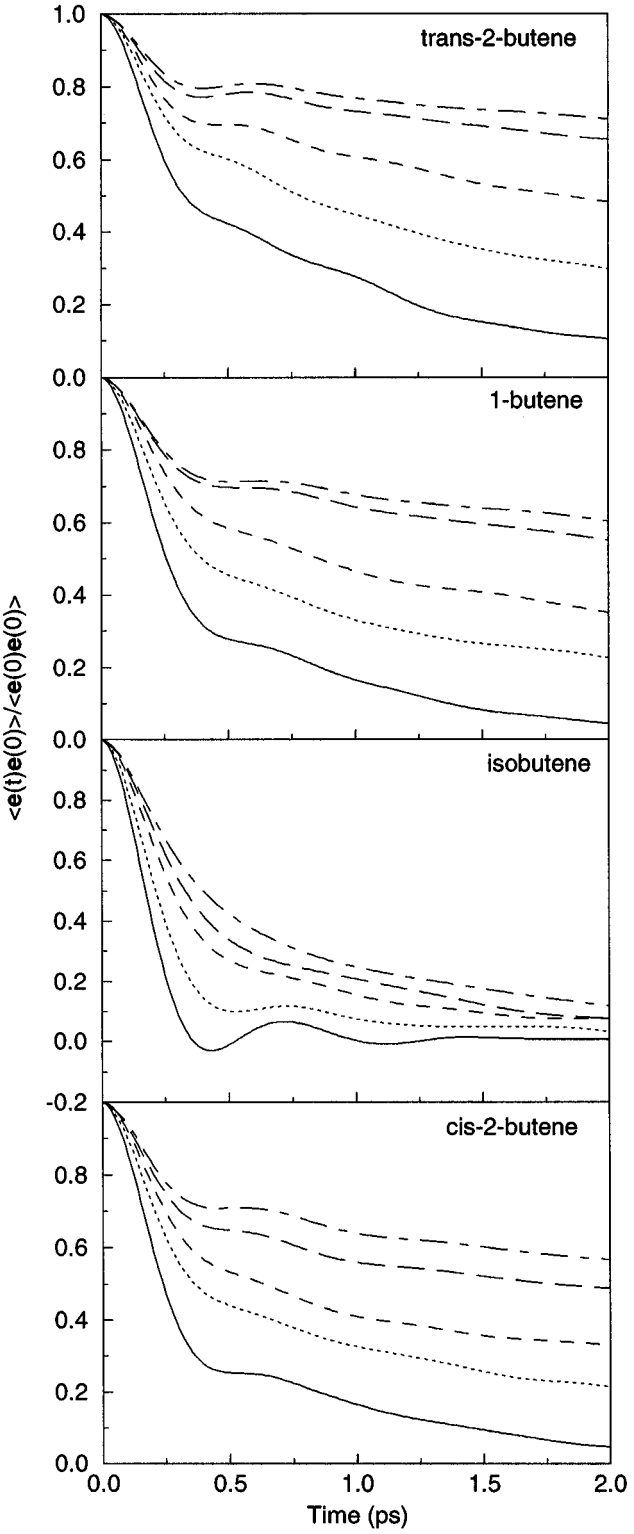

Figure 14. Orientational correlation function of the butene isomers in zeolite MEL, computed from MD trajectories at 623 K using the cff91_czeo force field of Biosym/MSI. Solid lines: zero loading. Dotted lines: 2.5 molecules/uc. Dashed lines: 5 molecules/uc. Long dashed lines: 7.5 molecules/uc. Dot dashed lines: 10 molecules/uc.

could be written as:

$$k_{ij}(n) = \alpha^n k_{ij}(0) \tag{8}$$

where $\alpha < 1$ is a unique parameter for all sites i and j, which is fitted against the MD results. This parameter influences the packing of the molecules in the sites and therefore is called the "steric factor". The maximum number of molecules that a given site can accommodate is evaluated from the MD trajectories

TABLE 4: Parameters of the Two-Sites JDM and Three-Sites CJDM of the Butene Isomers in Zeolite MEL at Nonzero Loading, Using as Input the Rate Constants Computed at Infinite Dilution and Given in Table 3[a]

	trans-2-butene	*cis*-2-butene	1-butene	isobutene
		2-Sites JDM		
N_S	4	1	1	
N_L	1	3	3	
α	0.6	0.1	0.2	
		3-Sites CJDM		
N_S	2	1	1	1
N_C	1	1	1	1
N_L	1	1	2	1
α	0.5		0.01	
χ	0.48	0.48	0.85	0.0

[a] N_Λ is the maximum number of molecules in site Λ, as computed from the MD trajectory with 20 molecules at 623 K, using the cff91_czeo force field of Biosym/MSI.

performed with 20 molecules, that is, 10 molecules/uc. They are listed in Table 4, together with the parameter α when necessary. The self-diffusivities derived from the JDM approach are compared graphically with the same values obtained from the MD runs in Figure 15.

There is a general good agreement between the diffusivities computed by molecular dynamics and by a jump diffusion model. Both the two-sites JDM and three-sites CJDM appear to reproduce reasonably well the evolution of the diffusivity of linear butene isomers in MEL as a function of the loading. A good agreement is also observed for isobutene using a three-sites JDM. Note that in all cases but isobutene, we have introduced an external bias to fit the diffusivities, either by the steric factor α for two-sites JDM or by the correlation factor χ for the three-sites JDM; however, these factors have a physical origin as they in fact give indications on the interactions of the guest molecules with the zeolite and with the other guest molecules. Indeed, we see that the steric factor for *trans*-2-butene is larger than for the other linear isomers, indicating that the interactions between the sorbed molecules are less repulsive for this isomer. In fact, the two-sites JDM and three-sites CJDM both underestimate the self-diffusivity of *trans*-2-butene at 2.5 molecules/uc; additional simulations suggested that the diffusivity could be larger at low loading ($\approx$1−2 molecules/uc) than at infinite dilution, indicating a preponderous effect of the interactions between the molecules, which was not taken into account in our present model. As the loading increases, the effect of the guest−guest intermolecular interactions becomes less important as the diffusion is limited by the blocking of the other molecules. As a general rule, the good agreement between the diffusivities computed by MD or JDM as a function of loading indicates that this blocking is the major process limiting the diffusion at medium or high loading.

The essential difference between the diffusion behavior of isobutene as compared to linear butenes, evidenced at infinite dilution by the good reproduction of the MSD derived from the MD trajectories by a three-sites JDM versus a two-sites JDM, respectively, appears to have a rather low influence on the diffusivities at higher loading. Indeed, the diffusion of linear butenes can also be modeled by a three-sites CJDM, which we have shown is no different from a normal JDM. This will allow us to conduct simulations with mixture of butene isomers, using the same model for all isomers, that is, a three-sites CJDM.

4. Conclusion

We have studied by molecular dynamics the self-diffusion of the four butene isomers in the all-silica form of zeolite types TON and MEL at 623 K. The results were compared with those

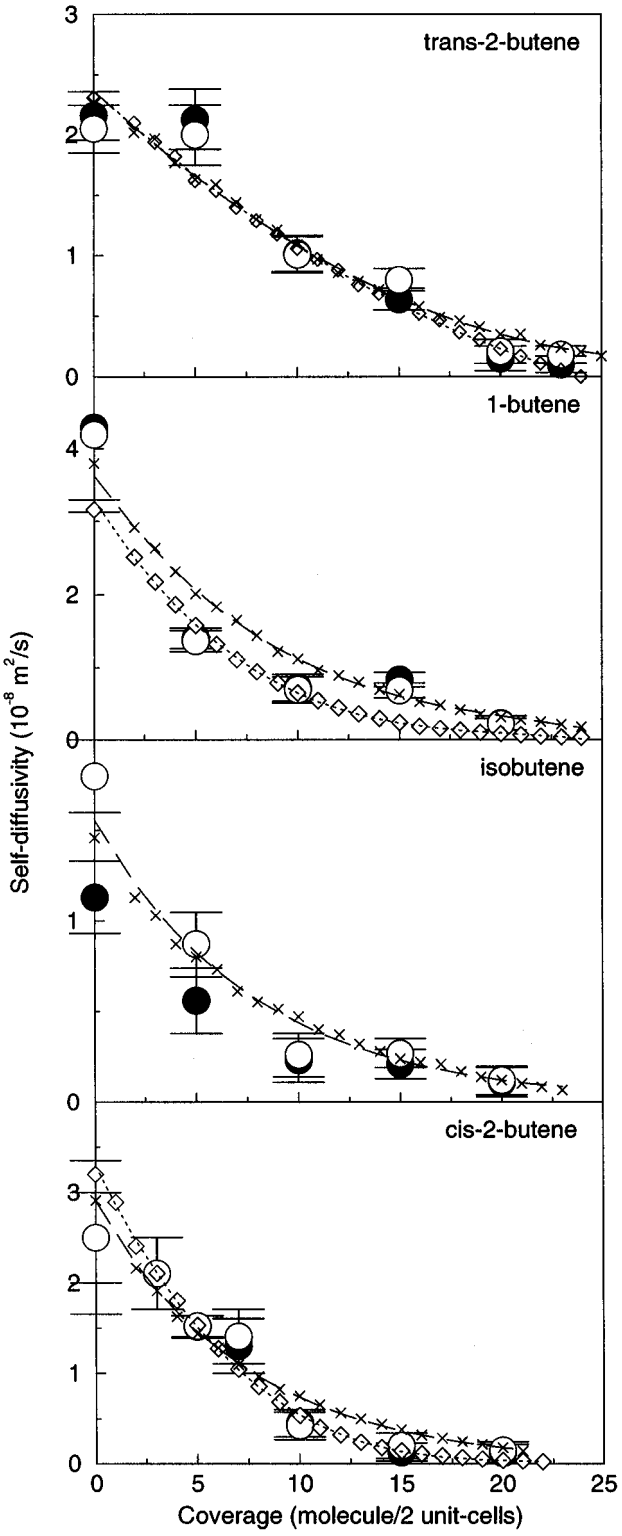

Figure 15. Self-diffusivities of the butene isomers in zeolite MEL at 623 K, as a function of the number of molecule in the model; circles are results of MD simulations using the force field cff91_czeo of Biosym/MSI (black circles: estimation from the MSD; white circles: estimation from the VACF; the error bars represent only statistical errors in the derivation of *D*); diamonds and dotted lines: from a two-sites JDM, using the transition probabilities computed at zero loading as input; crosses and dashed lines: from a three-sites CJDM.

derived from a jump diffusion model, to test the ability of a JDM approach to reproduce the main features of the diffusion of butene in those two zeolites.

Zeolite MEL presents three types of intrinsic sites where the short-time motions of the four butene isomers are different, as evidenced by the vibrational density of states. However, in the case of linear butenes, only the two sites corresponding to the two types of intersections are needed to model their diffusive behavior, while for isobutene all three sites have to be considered. As the intersections correspond to energy maxima, this shows the high influence of the entropy barrier for the high temperature considered here which inverts the free energy barrier at 623 K as compared to the energy barrier at 0 K. The general good agreement between the self-diffusivities computed by molecular dynamics and by a jump diffusion model in zeolite MEL indicates that this model can be used to represent the effects on the diffusivities of phenomena taking place on a larger spatial or time scale, such as pore blocking or crystallite size. It is likely that a similar model could be applied to related zeolites such as MFI or mordenite.

In the case of zeolite TON, the lower energy barriers and the absence of strong entropy barrier result in a poor fit of the diffusivities by a jump diffusion model. The introduction of a correlated jump diffusion model, where we assume that a given molecule has a larger probability to jump in the same direction as its previous jump than in the reverse direction improves the results, as it allows us to reproduce well the self-diffusivity and the mean-square displacement of isobutene and *cis*-2-butene, but not of *trans*-2-butene or 1-butene. For the latter two isomers, the influence of the guest−guest intermolecular interactions seems large at nonzero loading.

The intermolecular interactions also seem to influence profoundly the diffusion of *trans*-2-butene in zeolite MEL, as the self-diffusivities computed at low loading are larger than at infinite dilution; further investigations are needed to confirm this observation. At higher loading, the blocking due to the additional molecules becomes the major process limiting the diffusion and, therefore, the self-diffusivities computed by JDM agree well with those derived from the MD simulations. We think that it should be possible to incorporate the influence of the molecular interactions in the JDM, by considering different rate constants $k_{ij}(n_i,n_j)$ depending on the occupancy of the original site n_i and of the final site n_j. Of course this demands further simulations at low loading to get enough data to which this JDM approach could be compared; those aspects are currently under study.

A three-sites correlated jump diffusion model allows the simulation of the four butene isomers in zeolite MEL using the same network of sites. Hence, it becomes possible to study the diffusion of mixtures of all isomers in MEL with a unique approach. Moreover, we could include pore blocking and isomerization reactions within the same model. This would allow the simulation of a "realistic" system in conditions close to catalytic experiments, in a cheap and easy-to-do way, which is the ultimate goal of this theoretical study.

Acknowledgment. All authors wish to thank the FUNDP for the use of the Namur Scientific Computing Facility Center (SCF). They acknowledge financial support of the FNRS-FRFC, the "Loterie Nationale" for the convention No. 9.4593.92, the FNRS within the framework of the "Action d′impulsion à la recherche fondamentale" of the Belgian Ministry of Science under the convention No. D.4511.93, IBM Belgium for the Academic Joint Study on "Cooperative Processing for Theoretical Physics and Chemistry", and Biosym/MSI for the use of their software in the framework of the "Catalysis and Sorption" consortium. F.J. acknowledges Prof. A. Lucas, Director of the PAI 3-49, and the European Union for the attribution of a postdoctoral fellowship in the framework of the HCM/Host Institution ERB CHBG CT930343 "Science of Interfacial and

Mesoscopic Structures". L.L. thanks the FNRS for her position as a "Chargé de Recherches".

Appendix A: Multisite Transition Probabilities

The algorithm chosen for the jump diffusion model requires the computation of the probability for a given molecule to perform multiple jumps during a single time increment $\Delta\tau$. This can be calculated in the following way.

The probability for a molecule to reach a site i starting from a site 0 and following a given path $0 \rightarrow 1 \rightarrow 2 \rightarrow \cdots \rightarrow i$ can be described by the following differential equation system:

$$\begin{cases} \dot{p}_0 = -k_0 p_0 \\ \dot{p}_1 = -k_1 p_1 + k_{01} p_0 \\ \vdots \\ \dot{p}_i = -k_i p_i + k_{i-1,i} p_i \end{cases} \tag{A1}$$

where $p_0(0) = 1$, $p_i(0) = 0, i \neq 0$, $k_i = \sum_j k_{ij}$ is the total rate constant to get out of the site i, and $p_i(\Delta\tau)$ represents the probability to finally reach site i during $\Delta\tau$. This can be computed from the successive probabilities to jump out of site 0 and to a neighboring site 1, then out of site 1 to a neighboring site 2, etc. At each step the probability g_j to stay in site j is computed. A jump is attempted according to this probability, and if it is successful, the molecule moves to site $j+1$ according to the probability $k_{j,j+1}/k_j$. Hence, the final probability to reach site i is expressed as

$$p_i = \frac{k_{01}}{k_0}(1-g_0) \times \frac{k_{12}}{k_1}(1-g_1) \times \cdots \times \frac{k_{i-1,i}}{k_i - 1}(1-g_{i-1}) \times g_i \tag{A2}$$

Therefore, g_i is given by

$$g_i = p_i \frac{k_0 k_1 \cdots k_{i-1}}{k_{01} k_{12} \cdots k_{i-1,i}} (1-g_0)^{-1} \cdots (1-g_{i-1})^{-1} \tag{A3}$$

Still, the probability p_i has to be determined from eq A1. This system is rather simple to solve, but the analytical result has a different form if the rate constants are the same or not. Writing

$$\alpha_i = p_i \frac{k_0 k_1 \cdots k_{i-1}}{k_{01} k_{12} \cdots k_{i-1,i}} \tag{A4}$$

eq A1 becomes:

$$\begin{cases} \dot{\alpha}_0 = -k_0 \alpha_0 \\ \dot{\alpha}_1 = -k_1 \alpha_1 + k_0 \alpha_0 \\ \vdots \\ \dot{\alpha}_i = -k_i \alpha_i + k_{i-1} \alpha_i \end{cases} \tag{A5}$$

As a general rule, α_i can be written as a sum over all different transition probabilities k_j of a polynom of the $(m_j - 1)$th degree in $k_j\Delta\tau$, where m_j is the number of times a given molecule has jumped according to this transition probability k_j:

$$\alpha_i = \sum_{k_j \neq k_i} \left(\sum_{l=0}^{m_j - 1} a_l^{i,k_j} (k_j \Delta\tau)^l \right) \exp(-k_j \Delta\tau) \tag{A6}$$

The coefficients a_l^{i,k_j} in eq A6 can easily be computed from the coefficients a_1^{i-1,k_j} for α_{i-1}, using the recurrence relations

$$k_j \neq k_i \begin{cases} l = m_j - 1: & a_{mi-1}^{i,k_j} = \dfrac{k_{i-1}}{k_i - k_j} a_{mi-1}^{i-1,k_j} \\ l < m_j - 1: & a_l^{i,k_j} = \dfrac{k_{i-1}}{k_i - k_j} \left[a_l^{i-1,k_j} - \dfrac{k_j}{k_{i-1}} (l+1) a_{l+1}^{i,k_j} \right] \end{cases} \tag{A7}$$

$$k_j = k_i \begin{cases} l = 1, \ldots m_i: & a_l^{i,k_i} = \dfrac{k_{i-1}}{k_i} \dfrac{1}{l} a_{l-1}^{i-1,k_i} \\ l = 0: & a_0^{i,k_i} = -\sum\limits_{k_j \neq k_i} a_0^{i,k_j} \end{cases}$$

Appendix B: Correlated Jump Diffusion

In this Appendix is derived the expression of the propagator $P(r,t)$ for a model of correlated jump diffusion, that is, when a given molecule has a larger probability to jump in the same direction as its previous jump than in the reverse direction. Only the simplest case is considered here, that is, diffusion along a path of identical sites at infinite dilution. The propagator can be expressed as $P(n_R,n_L)$, where $n_R = {}^1/_2(N + r)$ is the number of jump that the molecule performs to the right and $n_L = {}^1/_2(N - r)$ is the number of jumps to the left. Considering a series of n sequences, where each sequence is composed of n_i jumps in the same direction, the probability to observe this given series, with fixed values of n_R and n_L, is simply

$$p(n) = \frac{1}{2p_2} p_1^N \left(\frac{p_2}{p_1} \right)^n \tag{B1}$$

where p_1 is the probability to jump in the same direction and $p_2 = 1 - p_1$ is the probability to jump in the reverse direction. Hence, $p(n)$ depends not on the number of jumps in a given direction but only on the total number of jumps N. Noting $C(n,n_R,n_L)$ the number of possibilities to have a series of n sequences with n_R and n_L fixed the (unnormalized) propagator becomes

$$P(n_R,n_L) = \sum_n p(n)\, C(n,n_R,n_L) = A \sum_n C(n,n_R,n_L) \alpha^n \tag{B2}$$

where A is a normalization constant and $\alpha = p_2/p_1$. The calculation of $C(n,n_R,n_L)$ varies with the following four different situations:

(1) There is an even number of sequences $n = 2p$ and the initial jump is to the right. Then, there are p sequences with jumps to the right, and p sequences with jumps to the left. $C(n,n_R,n_L)$ is simply the number of ways to put n_R red balls in p distinct boxes and n_L identical green balls in p distinct boxes, that is

$$C(n,n_R,n_L) = \binom{n_R - 1}{n_R - p} \times \binom{n_L - 1}{n_L - p} \tag{B3}$$

To simplify, suppose that $n_R > n_L$, that is, $r > 0$. Then, there are a maximum of n_L sequences for p.

(2) If the initial jump is on the right but there is an odd number of sequences $n = 2p + 1$, then

$$C(n,n_R,n_L) = \binom{n_R - 1}{n_R - p - 1} \times \binom{n_L - 1}{n_L - p} \tag{B4}$$

If $n_R > n_L$, there are also n_L sequences at most for p.

(3) If the initial jump is on the left but there is an odd number of sequences $n = 2p + 1$, then

$$C(n,n_R,n_L) = \binom{n_R - 1}{n_R - p} \times \binom{n_L - 1}{n_L - p - 1} \quad \text{(B5)}$$

If $n_R > n_L$, there are n_L-1 sequences at most for p.

(4) If the initial jump is on the left and there is an even number of sequences, then the expression is identical with the first case. As a result, the propagator for $r > 0$ is

$$P(n_R,n_L) = A(N,\alpha)\left\{2\sum_{p=1}^{n_L}\binom{n_R - 1}{n_R - p}\binom{n_L - 1}{n_L - p}\alpha^{2p} + \sum_{p=1}^{n_L}\binom{n_R - 1}{n_R - p - 1}\binom{n_L - 1}{n_L - p}\alpha^{2p+1} + \sum_{p=1}^{n_L-1}\binom{n_R - 1}{n_R - p}\binom{n_L - 1}{n_L - p - 1}\alpha^{2p+1}\right\} \quad \text{(B6)}$$

Writing $s = n_R$ - 1, $m = n_L$-1, and $k = p$-1, the preceding equation becomes

$$P(m,s) = B(N,\alpha)\left\{2\sum_{k=0}^{m}\binom{s}{k}\binom{m}{k}\alpha^{2k} + \sum_{k=0}^{m}\binom{s}{k+1}\binom{m}{k}\alpha^{2k+1} + \sum_{k=0}^{m-1}\binom{s}{k}\binom{m}{k+1}\alpha^{2k+1}\right\} \quad \text{(B7)}$$

If $n_R < n_L$, the same expression is obtained, where m and s are exchanged. This last expression can be written in terms of hypergeometric functions:

$$P(m,s) = B(N,\alpha)(2F(-m,-s;1;\alpha^2) + \alpha s F(-m,-s+1;2;\alpha^2) + \alpha m F(-m+1,-s;2;\alpha^2)) \quad \text{(B8)}$$

which can now be used to investigate its behavior at small times, or at large distances from the origin: indeed, the usual simplifying assumption that $r \ll N$ cannot be applied when $\alpha \to 0$, that is, the molecule has a much larger probability to jump always in the same direction. However, this approximation holds when only small correlations are considered. As $\alpha < 1$, when m and s become large, the terms with $k \to m$ in the expression B7 will not mean much as compared to the lowest or medium terms. Therefore, the following approximation can be made:

$$\binom{m}{k} \approx \frac{m^k}{k!} \quad \text{(B9)}$$

and the sum can be extended to infinity. This leaves:

$$P(m,s) \approx B(N,\alpha)\left(\sum_{k=0}^{\infty}\left\{2\frac{m^k s^k \alpha^{2k}}{k!k!} + \frac{m^k s^{k+1}\alpha^{2k+1}}{k!(k+1)!} + \frac{m^{k+1}s^k\alpha^{2k+1}}{(k+1)!k!}\right\}\right)$$

$$\approx B(N,\alpha)\left(2I_0(2\alpha\sqrt{ms}) + \left(\sqrt{\frac{s}{m}} + \sqrt{\frac{m}{s}}\right)I_1(2\alpha\sqrt{ms})\right) \quad \text{(B10)}$$

where I_0 and I_1 denote modified Bessel functions: $I_\nu(z) = e^{-i\nu\pi/2}J_\nu(ze^{i\pi/2})$. With the approximation, valid for N large and r not so large, that

$$\begin{cases} m \approx n_L = {}^1/_2(N + r) \\ s \approx n_R = {}^1/_2(N + r) \\ \epsilon = \dfrac{r}{N} \ll 1 \end{cases}$$

P can be written as

$$P(N,r) = 2B(N,\alpha)(I_0[\alpha N(1 - \epsilon^2/2)] + I_1[\alpha N(1 - \epsilon^2/2)]) \quad \text{(B11)}$$

Using the asymptotic expression of $J_\nu(z)$ for large arguments:[47]

$$I_\nu(z) \to \frac{1}{\sqrt{2\pi z}}\exp z \quad \text{(B12)}$$

equation B11 becomes

$$P(N,r) = C(N,\alpha)\exp\left(-\frac{r^2\alpha}{2N}\right) \quad \text{(B13)}$$

Replacing r by $R = lr$ and N by $t = N\tau$, this expression gives after normalization to unity

$$P(t,R) = \left(\frac{2\alpha\tau}{\pi l^2 t}\right)^{1/2}\exp\left(-\frac{R^2\tau\alpha}{2l^2 t}\right) \quad \text{(B14)}$$

When $\alpha > 1$, the same simplifying approximations can be used, provided that the index p in eq B7 is changed to $m - p$. Then, eq B14 is also obtained for $\alpha > 1$.

This last expression is formally identical with a normal random walk, where the step length l is replaced by $l/\sqrt{\alpha}$; that is, the behavior is identical with normal Fickian diffusion, with larger step if $\alpha < 1$ and smaller ones if $\alpha > 1$. Consequently, the mean-square displacement (MSD), which is the second moment of the propagator, is

$$\langle|R(t) - R(0)|^2\rangle = \int_0^\infty R^2 P(R,t)\,dR = \frac{2l^2 k}{\alpha}t \quad \text{(B15)}$$

where the transition probability $k = (2\tau)^{-1}$ have been introduced.

A short comment should be made about the behavior for noninfinite dilution in the single-file regime, that is, when the molecules are unable to pass each other. It is well-known that, for a random-walk process in the single-file regime, the mean-square displacement is proportional to the square root of time, rather than to time itself. Hahn et al.[6] have derived a formalism allowing to calculate the MSD in the single-file regime from the free propagator. As the propagator for correlated jumps is formally identical with that of a normal random walker, the corresponding MSD is also proportional to the square root of time. However, it has been shown by Kärger and co-workers[6,42] that in the case of molecules in the single-file regime, which change velocity only when encountering other molecules, the MSD becomes proportional to time. This corresponds to the extreme case of the correlated jump diffusion presented here at infinite dilution. Therefore, B14 does not hold for very high correlations, where eq B8 should be used instead.

References and Notes

(1) Breck, D. W. *Zeolite Molecular Sieves*; J. Wiley: New York, 1974.
(2) Barrachin, B.; Cohen de Lara, E. *J. Chem. Soc., Faraday Trans. 2* **1986**, *82*, 1953.
(3) Corma, A. *Chem. Rev.* **1995**, *95*, 559.
(4) Kärger, J.; Ruthven, D. M.; *Diffusion in Zeolites and other Microporous Solids*; J. Wiley: New York, 1992.
(5) Nelson, P.; Wei, J. *J. Catal.* **1992**, *136*, 263.
(6) Hahn, K.; Kärger, J. *J. Phys. A: Math. Gen.* **1995**, *28*, 3061.

(7) Leherte, L.; André, J.-M.; Derouane, E. G.; Vercauteren, D. P. *Int. J. Quantum Chem.* **1992**, *42*, 1291 and references therein.

(8) Schrimpf, G.; Schlenkrich, M.; Brickmann, J.; Bopp, P. *J. Chem. Phys.* **1992**, *96*, 7404.

(9) Dong, W.; Luo, H. *Phys. Rev. E* **1995**, *52*, 801.

(10) Ruthven, D. M.; Derrah, R. I. *J. Chem. Soc., Faraday Trans. 1* **1972**, *74*, 2332.

(11) June, R. L.; Bell, A. T.; Theodorou, D. N. *J. Phys. Chem.* **1991**, *95*, 8866.

(12) Auerbach, S. M.; Henson, N. J.; Cheetham, A. K.; Metiu, H. I. *J. Phys. Chem.* **1995**, *99*, 10600. Auerbach, S. M.; Bull, L. M.; Henson, N. J.; Metiu, H. I.; Cheetham, A. K. *J. Phys. Chem.* **1996**, *100*, 5923. Auerbach, S. M.; Metiu, H. I. *J. Chem. Phys.* **1996**, *105*, 3753.

(13) Mosell, T.; Schrimpf, G.; Brickmann, J. *J. Phys. Chem.* **1996**, *100*, 4582.

(14) Chandler, D. *J. Chem. Phys.* **1978**, *68*, 2959.

(15) Voter, A. F.; Doll, J. D. *J. Chem. Phys.* **1985**, *82*, 80.

(16) Theodorou, D.; Wei, J. *J. Catal.* **1983**, *83*, 205.

(17) Rödenbeck, C.; Kärger, J.; Hahn, K. *J. Catal.* **1995**, *157*, 656.

(18) Hernández, E.; Catlow, C. R. A. *Proc. R. Soc. London A* **1995**, *448*, 143.

(19) Meier, W. M.; Olson, D. H. *Atlas of Zeolite Structures Types*, 3rd ed.; Butterworth-Heinemann: London, 1992.

(20) Harrison, J. D.; Leach, H. F.; Whan, D. A. *Zeolites* **1987**, *7*, 21.

(21) Natarajan, S.; Wright, P. A.; Thomas, J. M. *J. Chem. Soc., Chem. Commun.* **1993**, 1861.

(22) Simon, M. W.; Suib, S. L.; O'Young, C.-L. *J. Catal.* **1994**, *147*, 484.

(23) Bianchi, D.; Simon, M. W.; Nam, S. S.; Xu, W.-Q.; Suib, S. L.; O'Young, C.-L. *J. Catal.* **1994**, *145*, 551.

(24) O'Young, C.-L.; Xu, W.-Q.; Simon, M.; Suib, S. L. In Weitkamp, J., Karge, H. G., Pfeifer, H., Hölderich, W., Eds. *Stud. Surf. Sci. Catal.* **1994**, *84*, 1673.

(25) Highcock, R. M.; Smith, G. W.; Wood, D. *Acta Crystallogr. C* **1985**, *41*, 1391.

(26) Marler, B. *Zeolites* **1987**, *7*, 393.

(27) Fyfe, C. A.; Gies, H.; Kokotailo, G. T.; Pasztor, C.; Strobl, H.; Cox, C. E. *J. Am. Chem. Soc.* **1989**, *111*, 2470.

(28) Terasaki, O.; Ohsuna, T.; Sakuma, H.; Watanabe, D.; Nakagawa, Y.; Medrud, R. C. *Chem. Mater.* **1996**, *8*, 463.

(29) Mosell, T.; Schrimpf, G.; Hahn, C.; Brickmann, J. *J. Phys. Chem.* **1996**, *100*, 4571.

(30) Discover User Guide, version 95.0; Biosym/MSI: San Diego, 1995.

(31) Hill, J.-R.; Sauer, J. *J. Phys. Chem.* **1994**, *98*, 1238. Hill, J.-R.; Sauer, J. *J. Phys. Chem.* **1995**, *99*, 9536.

(32) Jousse, F.; Leherte, L.; Vercauteren, D. P. *Mol. Simul.* **1996**, *17*, 175.

(33) Santikary, P.; Yashonath, S. *J. Phys. Chem.* **1994**, *98*, 9252.

(34) Smirnov, K. S. *Chem. Phys. Lett.* **1994**, *229*, 250.

(35) Allen, M. P.; Tildesley, D. J. *Computer Simulations of Liquids*; Clarendon Press: Oxford, 1987.

(36) Cao, P. L. *Phys. Rev. Lett.* **1994**, *73*, 2595.

(37) Hahn, K.; Kärger, J.; Kukla, V. *Phys. Rev. Lett.* **1996**, *76*, 2762.

(38) Kukla, V.; Kornatowski, J.; Demuth, D.; Girnus, I.; Pfeifer, H.; Rees, L. V. C.; Schunk, S.; Unger, K. K.; Kärger, J. *Science* **1996**, *272*, 702.

(39) Shen, D.; Rees, L. V. C. *J. Chem. Soc., Faraday Trans.* **1996**, *92*, 487.

(40) Jousse, F.; Leherte, L.; Vercauteren, D. P. *J. Mol. Catal.* **1997**, *119*, 165.

(41) van Beijeren, H.; Kehr, K. W.; Kutner, R. *Phys. Rev. B* **1983**, *28*, 5711.

(42) Hahn, K.; Kärger, J. *J. Phys. Chem.* **1996**, *100*, 316.

(43) Keffer, D.; McCormick, A. V.; Davis, H. T. *Mol. Phys.* **1996**, *87*, 367.

(44) Derouane, E. G.; André, J.-M.; Lucas, A. A. *J. Catal.* **1988**, *110*, 58.

(45) Derycke, I.; Vigneron, J. P.; Lambin, Ph.; Lucas, A. A.; Derouane, E. G. *J. Chem. Phys.* **1991**, *94*, 4620.

(46) IBM Visualization Data Explorer version 1.2 User's Guide; IBM Corp. (Ed.): Yorktown Heights, NY, 1992.

(47) Abramowitz, M.; Stegun, I. (Eds.) *Handbook of Mathematical Functions*, 9th ed.; Dover Publications: New York, 1970.